Chapter 3

Finite Element Modeling

3.1 Introduction and justification

This chapter introduces the background and details of the numerical models used to simulate the structures. Finite Element Analysis (FEA) is used to replicate the experimental investigation. Details for the model, including nonlinear material properties are explained. The results extracted from the experimental investigations, demonstrate that the behavior of the structures comprise material and geometric nonlinearities, including dynamic effects involved in the case of the concrete frame subjected to blast loads. The finite element models can replicate the response of the full scale concrete model to an extreme event and provide accurate results of the damage sustained and the potential for progressive failure of the structures. A full scale FEA model require long computational times and large amounts of memory and sometimes models experience convergence issues, especially in the non linear analysis. But due to the limitations of other methods, the advantages of the finite element analysis are clearly superior and shall be used to conduct the investigations.

3.2 Description of the model

3.2.1 Two-story concrete slab with corner column removal

3.2.1.1 Geometry of the model

The FEM model consists, as well of the experimental model, of two 25 cm slabs with external dimensions of 7x7 m^2, supported on 4 columns with spans of 6.60 m. The height of the columns is 2.5 m with a section of 25x25 cm^2 reinforced concrete elements.The reinforcement consists in a 16 mm bar mesh spaced at 20 cm placed on the bottom of face and a 12 mm

bar mesh spaced at 20 cm placed on the top face. A supplementary reinforcement of 12 mm bars spaced at 20 cm is placed on the bottom face in the column strip (1/4 of the transversal span in the vicinity of the columns). The reinforcement of the supports consists in 4, 12 mm bars on the corners with 12 mm stirrups spaced at 10 mm in the top and bottom 50 cm and spaced at 20 cm in the central part of the supports.

3.2.1.2 Modeling of concrete

For the development of the finite element model, the explicit finite element software LS-DYNA Hallquis, 2016 is used due to its numerical stability and variety of constitutive models. Eight node solid hexahedron elements are used to simulate concrete parts. In this study, the CSCM model is used to simulate the concrete behavior. This material model can achieve stable results and several researches have proven its accuracy in the simulation of reinforced concrete subjected to sudden column removal Pham et al., 2017. This model is isotropic and has different response in tension and compression, three plasticity surfaces, softening in compression, damage in tension, and erosion formulation for the elimination of material. This concrete model in LS-DYNA is provided based on three input specifications: the unconfined compression strength, the aggregate size, and the units. The unconfined compression strength affects stiffness, strength, hardening, and softening. The CSCM model is valid for normal compressive strengths from 28 MPa to 58 MPa. The aggregate size affects the brittleness of the softening behavior of the damage formulation Murray, 2004.
Table 3.1 shows the parameters used for the material model *MAT_CSCM_CONCRETE.

Table 3.1: Parameters used for *MAT_CSCM_CONCRETE

Parameters	LS-DYNA Symbol	Value
Mass density	RO	2300 kg/m^3
Erode Parameter	ERODE	1.1
Unconfined compression strength	FPC	30 MPa
Maximum aggregate size	DAGG	20 mm

3.2.1.3 Modeling of steel reinforcement

The reinforced bars are modeled explicitly using two node Hughes-Liu beam elements with 2x2 Gauss points in the cross section and located in the exact position within the concrete mesh with a circular cross section with different diameters. Each beam element contained two nodes. The steel behavior is represented using the Piecewise Linear Plasticity material model, which is an elastoplastic material model with hardening, equal response in tension and compression, and failure when the effective plastic strain reaches the ultimate strain.

Table 3.2: Parameters used for Piecewise Linear Plasticity material model for steel rebars

Parameters	LS-DYNA Symbol	Value
Mass density	RO	7850 kg/m^3
Young's modulus	E	210 GPa
Poisson's ratio	PR	0.3
Yield stress	SIGY	500 MPa
Tangent modulus	ETAN	422 MPa
Effective plastic strain to failure	FAIL	0.075

LS-DYNA provides different solid element formulations. One integration point at the center of the element is used for modeling concrete in this study. This solid element formulation has three translational degrees of freedom at each node.

Although a single point integration formulation is effective for modeling nonlinear material behavior and capturing large deformations, it does suffer from hourglassing or zero-energy modes. To avoid zero energy deformations, or hourglassing, an artificial stiffness is added to the eight node solid elements to resist these zero-energy deformation modes using *CONTROL_HOURGLASS in LS-DYNA.

The initial state of the structure under the gravity load is achieved though a dynamic relaxation state. Next, the fixed support at the bottom of the column is removed using birth and death technique, triggering the process.

Figure 3.1 shows details of the model where the size of the concrete elements as well as the modelling of the reinforcement can be seen. Figure 3.2 shows a global view of the LS-Dyna model.

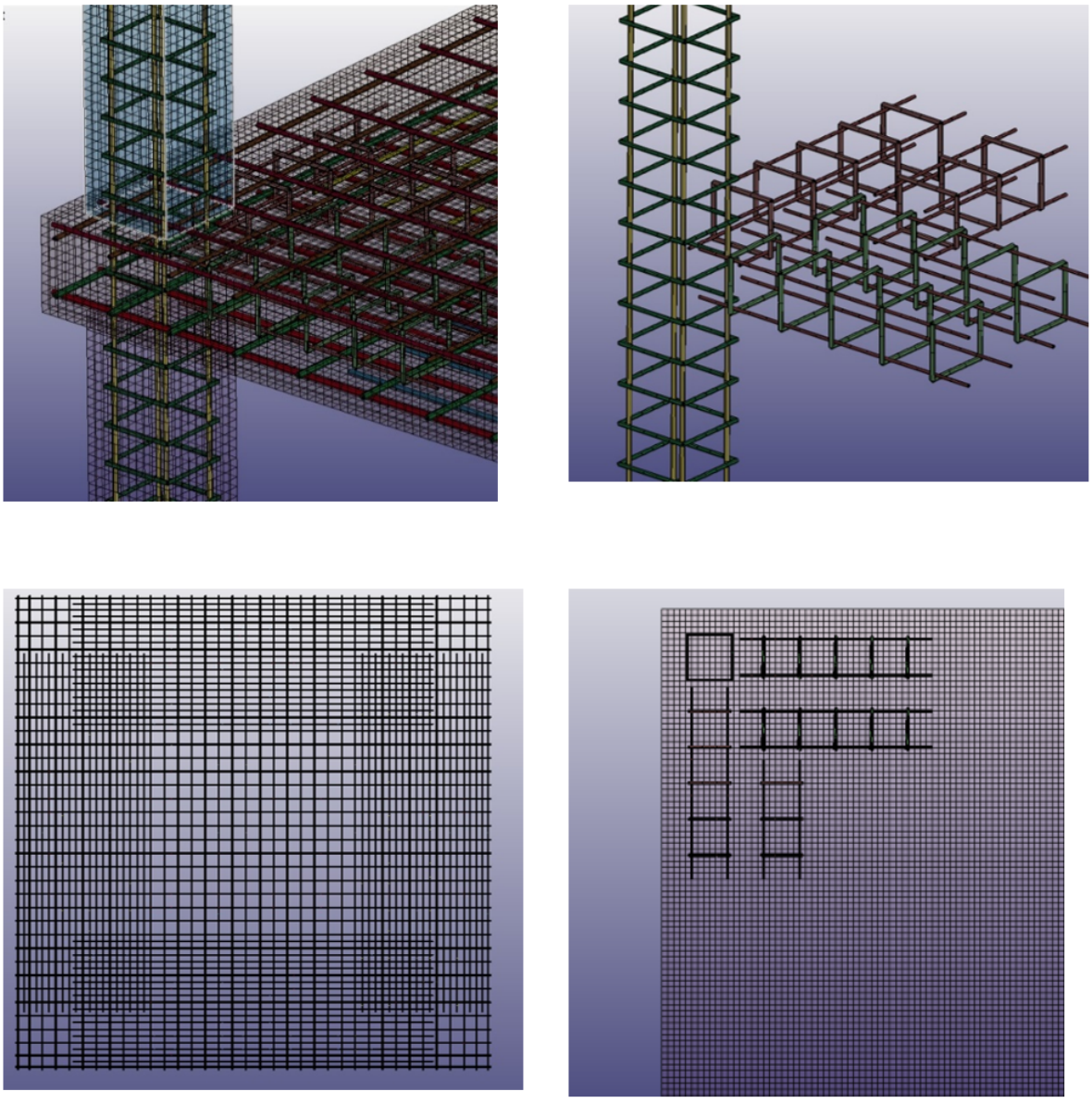

Figure 3.1: FEM model details

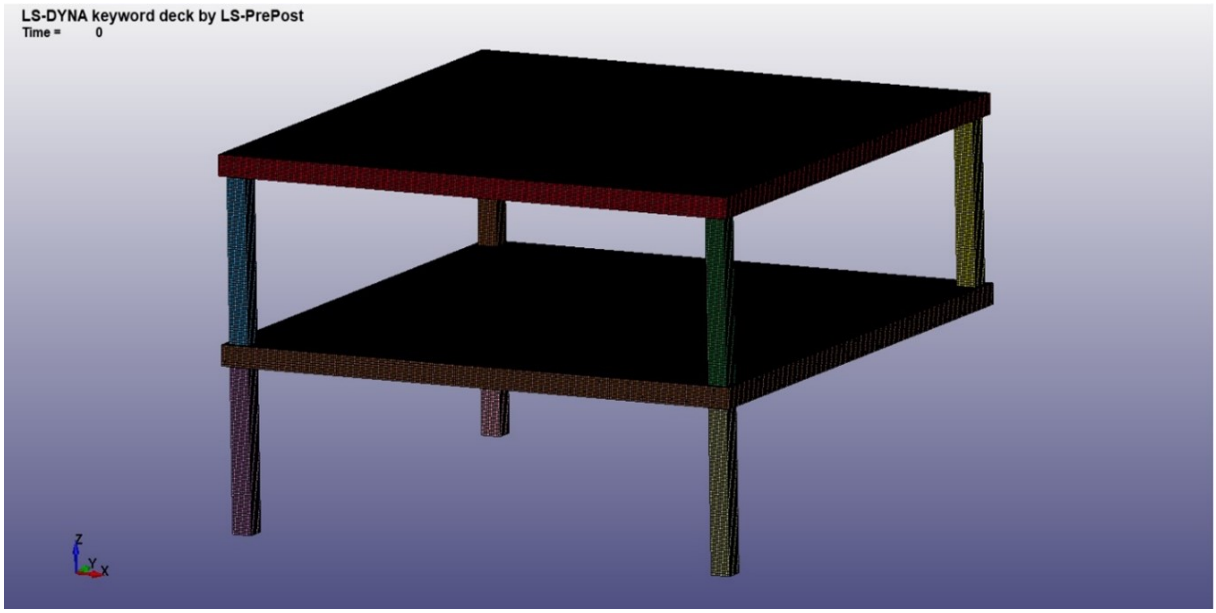

Figure 3.2: FEM model

3.2.1.4 Boundary conditions

To avoid interpenetration between the rebar beam elements during the large-deformation phase, the keyword *CONTACT_AUTOMATIC_GENERAL was used to simulate the interaction between the rebars. The translational constraints in the X, Y, and Z directions were assigned to each column at their bottom nodes of the concrete and rebar elements. To obtain the reaction forces during the simulation, the keyword *DATA_CROSS_SECTION_SET was defined. The simulation of the column removal is performed by replacing the column with a kinematic constraint that prevents movement at the bottom of the column for 0.5 seconds. This time is necessary for the dynamic relaxation to converge and the deformation due to the self-weight is reached. Once this time ended, the restriction on movement is abruptly eliminated, leaving gravity to act. The overload is included in the model by means of a distributed pressure applied on each of the upper faces of the elements. The other three columns are fixed at their base to simulate their union with the foundation. To connect the reinforcement and concrete *CONSTRAINED_LAGRANGE_IN_SOLID was used. Model fixed boundary conditions are applied at the bottom of each column.

3.2.1.5 Effect of mesh sensitivity analysis

Sensitivity analysis is a crucial step in computational mechanics and structural engineering and aims at quantifying the relative importance of each input parameter, potential interaction and the effects on the model response. To validate the size of the mesh of the FE model, three series of models with the same geometry and boundary conditions but different elements size were analyzed. The results of this three models were compared to the result obtained in the

real test. It can be observed that, the mesh size significantly affects the structural response. The deflection versus time relationship for the three mesh sizes displayed in Figure 3.3, and base on these results, the element size was decided as 25 mm for concrete and reinforcement, since this value provide the more accurate result comparing with the real test.

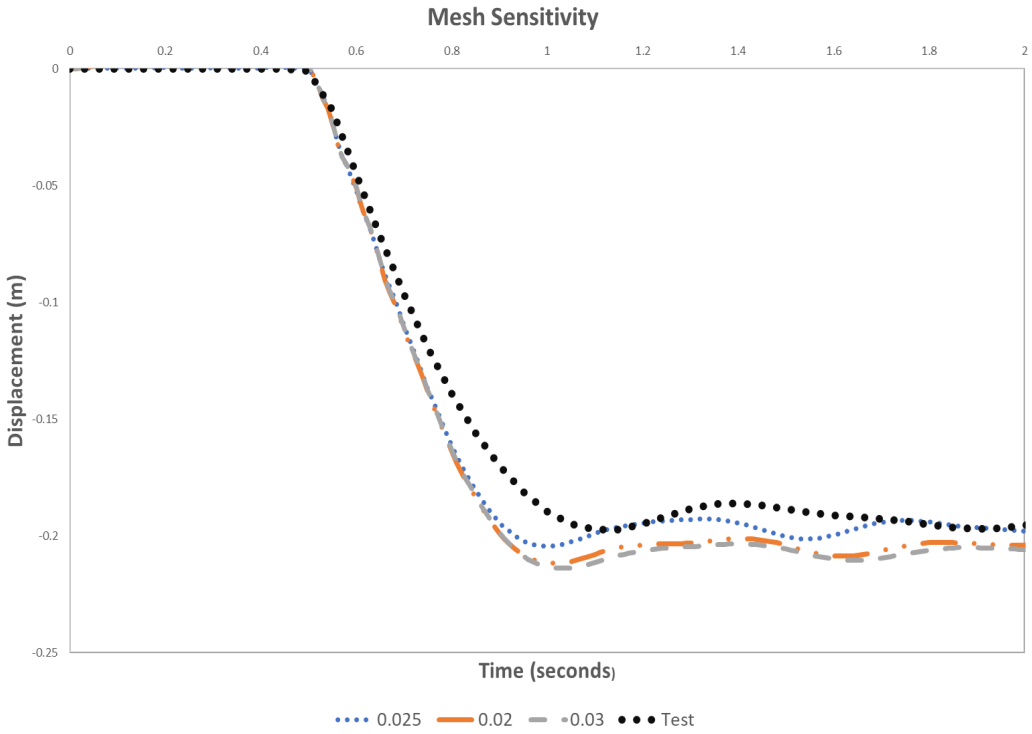

Figure 3.3: Mesh sensitivity analysis

3.2.2 Two-span concrete frame subjected to successive blast loads

3.2.2.1 Modeling of concrete

For the material model used for concrete, it is necessary to define the uniaxial tensile strength (UTS) together with the uniaxial compressive strength (UCS). In this case, the value has been calculated using the formula provided by EC2 as follows:

$$f_{ctm} = 0.30 \times f_{ck}^{\frac{2}{3}} \tag{3.1}$$

being ck for concrete class $\leq$ C50/60, being fck the characteristic compressive strength. Thus, in the simulations carried out to test the influence of the variation of the concrete compressive strength, the UTS values were modified accordingly being in these cases 2.56, 2.89 and 3.21 MPa respectively. As can be seen in 3.5, this parameter also has negligible influence on the simulation result. It can therefore be concluded that a 40% increase in the concrete strength values will hardly influence the simulation result. This is mainly due to the fact that the strength of the structure is provided by the steel reinforcement as the concrete

slabs work mostly in bending. The reinforcement steel is perfectly characterised and the model parameters are those showed in Table 3.4 and required according to the material model (*Piecewise_Linear_Plasticity).
Regarding the material model used for concrete, the Winfrith material model (MAT084) which was developed in the 1980s to solve RC structures subjected to impact loads and implemented in LS-DYNA in 1991, so it can be considered sufficiently tested. However, there are other material models included in LS-DYNA which work with simplified input parameters also offering good results. But, looking at the experimental results, after the first and second tests the damage was minimal. Only after the third test local damage was observed. The modification of the material model used for concrete would have an impact on a larger or smaller crater in the structure, but would not differ in anything else.
Another parameter that can have an influence on the simulation result is the hourglass technique used. LS-DYNA recommends viscous hourglass control for problems deforming with high velocities, as this is the case. Stiffness control is often preferable for lower velocities, especially if the number of time steps are large. Given the problems with using the standard LS-DYNA viscous form (i.e. IHQ = 1) for hourglass control in high strain rate problems, the option IHQ = 3 Flanagan-Belytschko viscous form with exact volume integration for solid elements has been chosen, since, as stated in the LS DYNA manual, for solid elements the exact volume integration provides some advantage for highly distorted elements.
As for the blast load, it was applied using the load blast enhanced (LBE) feature, which is an improved version of the Load Blast command.
The LBE technique is optimal when the explosive used is TNT or its equivalent is known. In this study, the pressures were measured in the three tests performed and the results were found to correspond to the detonated charges, and therefore the TNT equivalent masses were as initially calculated (10 kg TNT eq. for the first test and 20 kg TNT eq. for the second and third tests). The pressure was applied directly to the structure by defining a segment for the impact of the shock wave. To use the LBE technique, it is only necessary to define the equivalent mass of TNT and the charge coordinates. In addition, the type of blast source needs to be specified. In case of the third test where the local damage was observed, the type of source defined was hemispherical surface burst, which means that the charge is located on or very near the ground surface. Furthermore, the validity range of this option is determined by the scaled distances between 0.178 and 40 m/kg$^{1/3}$, and here, the test carried out was within this range.

In this case the Winfrith model is used for concrete. This model is based on the Ottosen plasticity model and allows modeling of softening of concrete in tension (through fracture Energy, allowing for aggregate size) and can account for strain rate. Eight node solid hexahedron elements are used to simulate concrete parts (Figure 3.4). As the Rate-Card of the Winfrith material is set to 0 LS-DYNA uses the specific fracture energy, i.e. energy per unit area dissipated in opening a crack. The fracture energy GF [N/m] is calculated using the equation:

$$G_F = 73 \times f_c^{0.18} = 137\frac{N}{m} \tag{3.2}$$

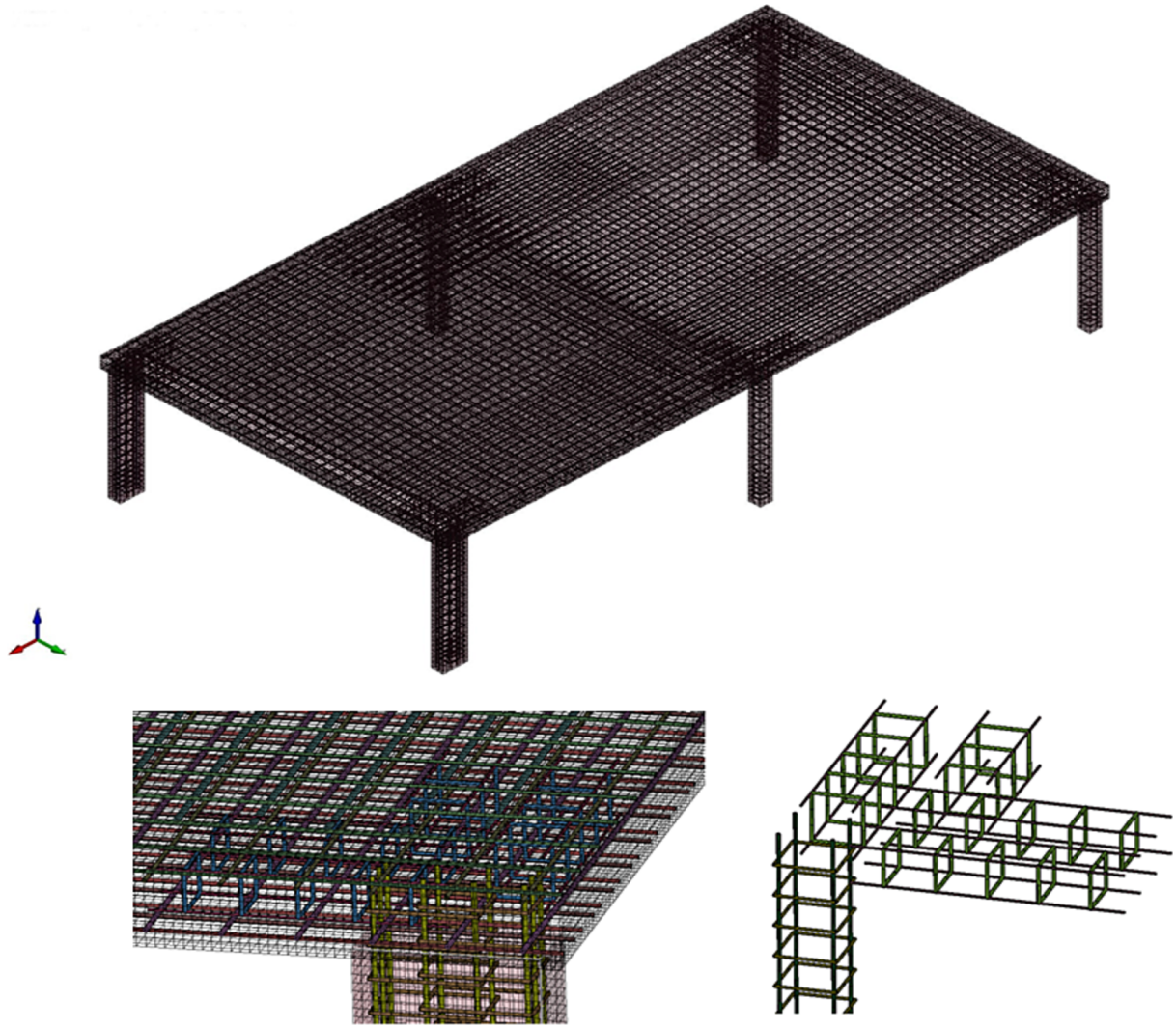

Figure 3.4: FEM model details.

For the model, the element size at the blast impact location is 0.05 m. If the mesh size is smaller than the fracture progress zone (FPZ) the model is affected by the fracture energy dissipation leading to a failure response of the whole structure (depending on the explosive charge and therefore the pressures applied to the structure) Khoe and Weerheijm, 2012, Alañón et al., 2018. The reinforced bars are modeled explicitly using two node Hughes-Liu beam elements with 2x2 Gauss points in the cross section and located in their theoretical position within the concrete mesh. Table 3.3 shows the parameters used for the material model for concrete *MAT_Winfrith. Note that, unfortunately, no tests of the concrete strength are available, so the design characteristic strength increase by 8 MPa, as recommended by EC2 Européen, 2004 was used as the mean concrete strength. This fact does not undermine the results of the model as the behavior of concrete is more influenced by other factors than the compressive strength of the concrete Grisaro, 2021.

Table 3.3: Parameters used for *MAT_Winfrith

Parameters	LS-DYNA Symbol	Value
Mass density	RO	2300 kg/m^3
Initial tangent modulus of concrete	TM	26.94 GPa
Unconfined compressive strength	UCS	33 MPa
Unconfined tension strength	UTS	3.3 MPa
Poisson´s ratio	PR	0.17
Aggregate size (radius)	ASIZE	0.01 m

3.2.2.2 Modeling of steel reinforcement

Steel behavior is represented using the Piecewise Linear Plasticity material model, which is an elastoplastic material model with hardening, equal response in tension and compression, and failure when the effective plastic strain reaches the ultimate strain. Table 3.2 listed the parameters used for Piecewise Linear Plasticity material model for steel rebars. For reinforcement, the steels manufactured in Spain are well characterized by the industry. The values used for the analysis fy = 500 MPa and a tangent modulus for the second line of the bilinear law of 1194 MPa are taken from data provided by the Spanish steel reinforcement manufacturing association for a steel of class B 500 SD.

Table 3.4: Parameters used for Piecewise Linear Plasticity material model for steel rebars

Parameters	LS-DYNA Symbol	Value
Mass density	RO	7850 kg/m3
Young's modulus	E	210 GPa
Poisson's ratio	PR	0.3
Yield stress	SIGY	500 MPa
Tangent modulus	ETAN	422 MPa
Effective plastic strain to failure	FAIL	0.11

LS-DYNA provides different solid element formulations. One integration point at the center of the element is used for modeling the concrete in this study. This solid element formulation has three translational degrees of freedom at each node. Although a single point integration formulation is effective for modeling nonlinear material behavior and capturing large deformations, it does suffer from hour glassing or zero-energy modes. To avoid zero energy deformations, or hour glassing, an artificial stiffness is added to the eight node solid elements to resist these zero-energy deformation modes using *CONTROL_HOURGLASS in LS-DYNA. The initial state of the structure under the gravity load is achieved through a dynamic relaxation state. The blast pressure can be automated in the LS-DYNA environment and applied on the blast-facing surface of the slab and columns using the *LOAD_BLAST_ENHANCED (LBE) keyword. This function is based on the Kingery-Bulmash empirical blast data Kingery and Bulmash, 1984. In this approach, the blast pressures on slab and supports were generated following the CONWEP empirical relations Hyde, 1992.
The element erosion function, while not a property or physics-based phenomenon, provides a

useful means of simulating the spalling of concrete and provides a more realistic graphical representation of blast events. Erosion is characterized by the physical deletion of the eroded solid element from the rest of the mesh Wu et al., 2011. The most common erosion criteria used are the instantaneous geometric strain and maximum principal strain. These criteria can be used to smooth simulations. The maximum strain criterion acts as a limit on tension strain. This criterion, when applied to brittle materials like concrete, can be physically interpreted as a lower limit on crack opening. Luccioni and Aráoz, 2011 summarized recent past research to show that the maximum principal strain can represent tensile fracture and spalling of concrete under blast and impact loads. Maximum principal strain values are often used as the erosion criterion in the simulation of concrete fracture and cracking Tanapornraweekit et al., 2008 Xu and Lu, 2006. Other criteria such as maximum tensile stress and maximum shear strain Teng et al., 2008 have also been used to simulate concrete damage. Maximum principal strain has been used is this study for spalling and damage assessment. To visualize the formation of the crater, an additional erosion criterion has been taken (which in LS-DYNA is introduced by means of the command *MAT_ADD_EROSION). Following the indications Luccioni and Aráoz, 2011, for concretes with the same order of element sizes and scaled distance similar to those used in this study, a value for the maximum principal strain at failure of 0.01 has been selected as a criterion.

3.2.2.3 Boundary conditions

Model fixed boundary conditions are applied at the bottom of each column. To avoid interpenetration between the rebars beam elements during the large-deformation phase, the keyword *CONTACT_AUTOMATIC_GENERAL was used to simulate the interaction between the rebars. The translational constraints in the X, Y, and Z directions were assigned to each column at their bottom nodes of the concrete and rebars elements. To obtain the reaction forces during the simulation, the keyword *DATA_CROSS_SECTION_SET was defined. To connect the concrete and steel reinforcement, *CONSTRAINED_LAGRANGE_IN_SOLID command was used.

3.2.2.4 Sensitivity analysis

In the numerical model there are a large number of parameters relating to blast type and material properties. All the parameters used have been selected according to the test to be modeled and some of them based on references of works in line with the present study. Therefore, this section aims to justify and clarify some of the assumptions made on model parameters.
As mention in Section 2.5.2.2 Chapter 2, no test were carried out to obtain the mechanical properties of the concrete. However, this value of compressive strength could not be necessarily the real value or even sufficiently close to the real value. In order to check that there are no noticeable differences when changing the concrete strength, different models have been run with compressive strengths of 25, 30 and 35 MPa. As can be seen in Figure 3.5, the residual displacement after the three tests run in series is practically the same, with a difference of 2 mm between the concrete with the highest and lowest strength. This displacement has been

evaluated at a node located in the center of span 1. Therefore, it can be concluded that in this case the influence of the concrete strength is negligible considering the tested loads and scaled distances

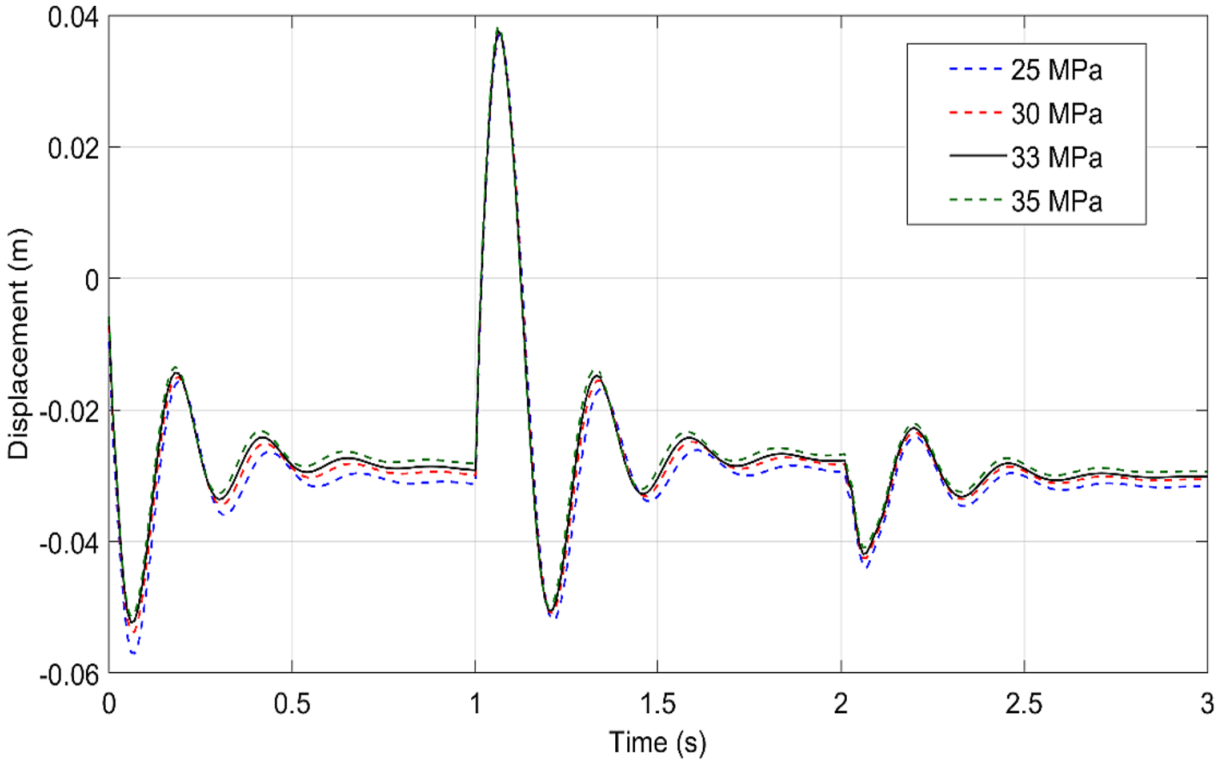

Figure 3.5: Residual displacement vs. time obtained with different values of compressive strength (25, 30, 33 and 35 MPa).

Chapter 4

Validation of the Finite Element Model

4.1 Introduction

The purpose of this chapter is validate the FE model against the results from the experimental test described in Section 2.5, Chapter 2. This Chapter does not aim to adjust material properties or modeling parameters to enhance alignment between numerical and experimental results. Rather, it utilizes the modeling approach outlined in Chapter 3, incorporating measured material properties and defined geometries, to compare finite element results with corresponding experimental outcomes. Consequently, all data collected, analyzed, and discussed in Chapter 2, Section 2.5 can be assessed alongside the numerical results, allowing observations on both similarities and differences. Given the inherent uncertainties in experimental investigations and the assumptions within the modeling process, an exact match between cases is neither anticipated nor necessary.

4.2 Validation of the FEM against experimental results

In this chapter, the FEM described in previous chapter is used to replicate the experimental investigation at UPM discussed in Chapter 2, Section 2.5. The results of both experiments and the FEM analysis are compared to validate the modeling assumptions.

4.2.1 Two-story concrete slab with corner column removal

4.2.1.1 Model validation

Figure 4.1 show a comparison between the deflections measured by laser-scan and the prediction of the model. It can be seen that both the shapes and values obtained by the simulation are

very close to those of the test.

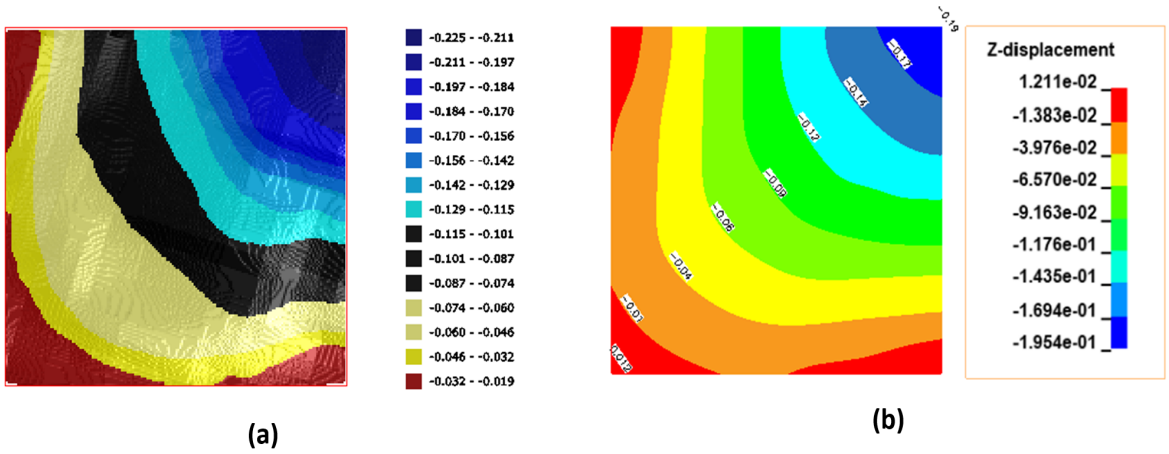

Figure 4.1: Test (a) and FEM (b) Top Slab Deflection.

It is also worth noting that the value of the maximum deflection is relatively low and not sufficient to generate significant membrane action. This explains why the simple linear-elastic model with cracked stiffness presented in Section 4.1 also obtained a good approximation to the observed deflections. Figure 4.2 shows a comparison between the time history of displacements measured by DIC and the prediction of the FEM model using a reasonable damping index of 2%. This damping ratio has been selected due to the relatively small damage observed on the specimen.

Cracks were small enough to be admissible in SLS. This damping index is within the range recommended by EN1991:2, 2003 for reinforced concrete railway bridges. It can be seen that there is good agreement between experimental and model results. A very interesting fact that can be derived from this figure is that the impact factor is quite low, as can be seen from the small magnitude of the oscillation of deflections after the collapse of the column. Reasons for this can be related to the asymmetry in stiffness as the slab is cracked when deflecting downwards, but not when deflecting upwards. Immediately after the sudden column removal, static equilibrium is not satisfied and the deflections become larger in order to increase the strain energy of the system.

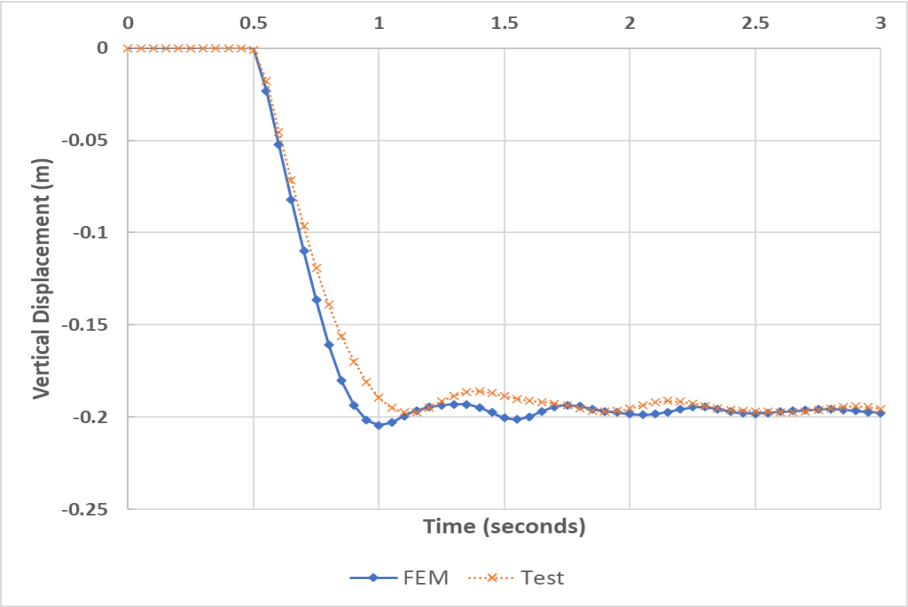

Figure 4.2: Comparison of the displacement history from FEM model and test results.

This excess of external work is transformed into kinetic energy, increasing the velocity of the structural system (see Figure 4.3).

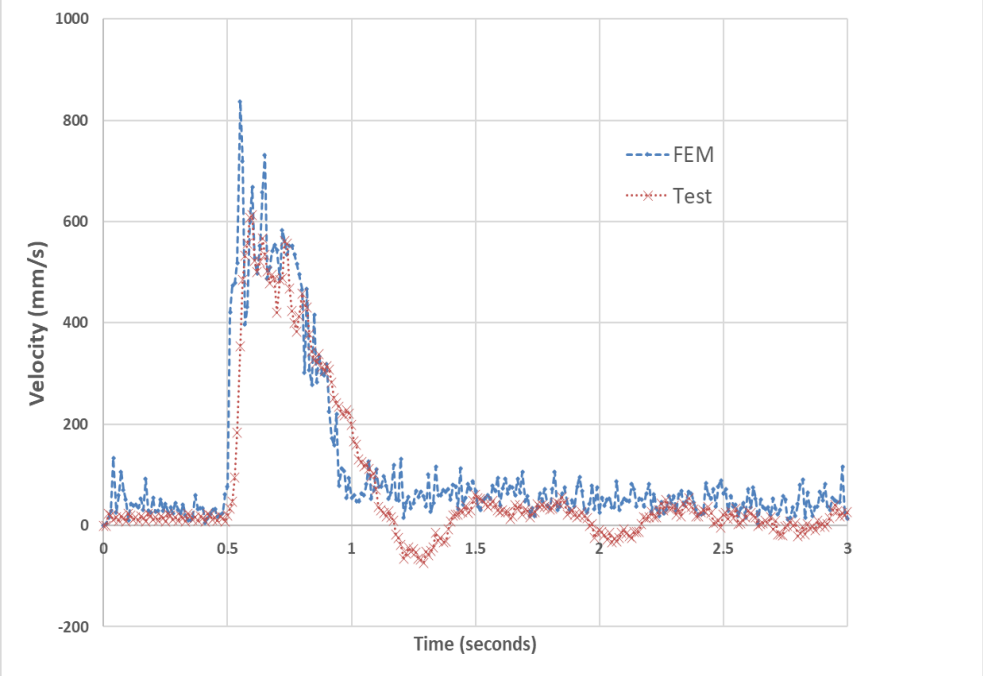

Figure 4.3: Velocity of corner of slab. Comparison between experimental values and values obtained by FEM. The test value is obtained by numerical derivation of the deflection results obtained by DIC.

As the structure deflects, the kinetic energy decreases, and the structure absorbs the potential energy of gravity loads in form of elastic and inelastic energy. The maximum dynamic response is reached when the work done by gravity loads is equal to the stored strain energy of the system, and hence the kinetic energy is zero (see Figure 4.4).

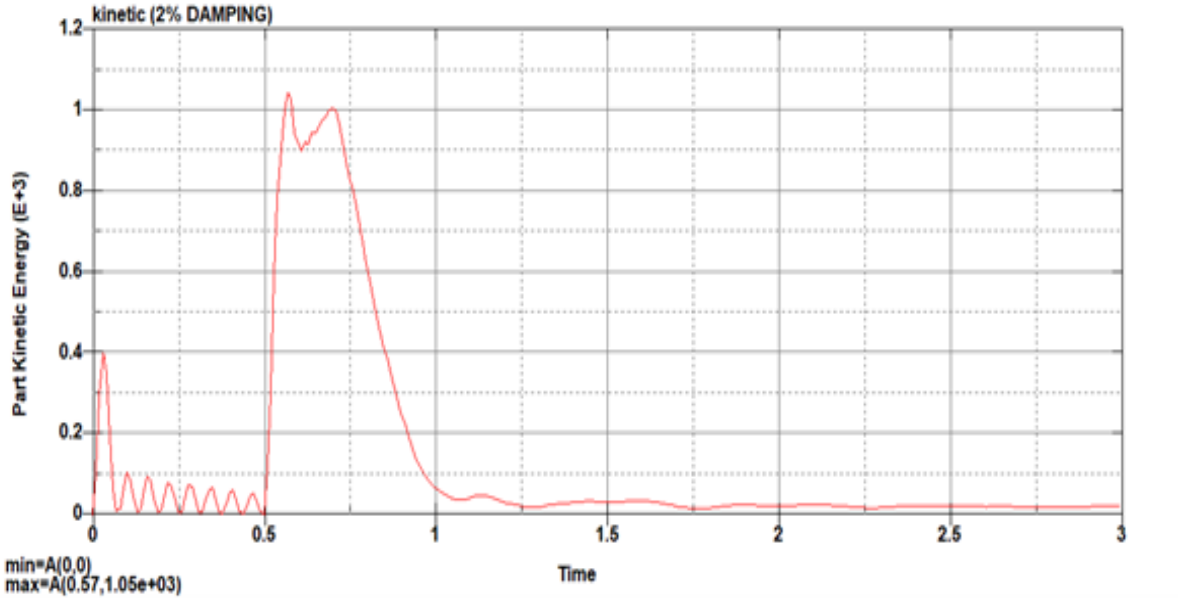

Figure 4.4: Kinetic Energy of the structure determined by FEM analysis for 2% damping.

Figure 4.5 to Figure 4.10 presents a comparison between the observerd damage at the end of the test and the peak tensile strain concentrations from the LS-Dyna model. Although the LS-Dyna concrete material model does not explicitly show the cracks that form on the surface, a reasonable approximation of crack location can be obtained by plotting the maximum principal strain at the solid integration points used to model the concrete material.

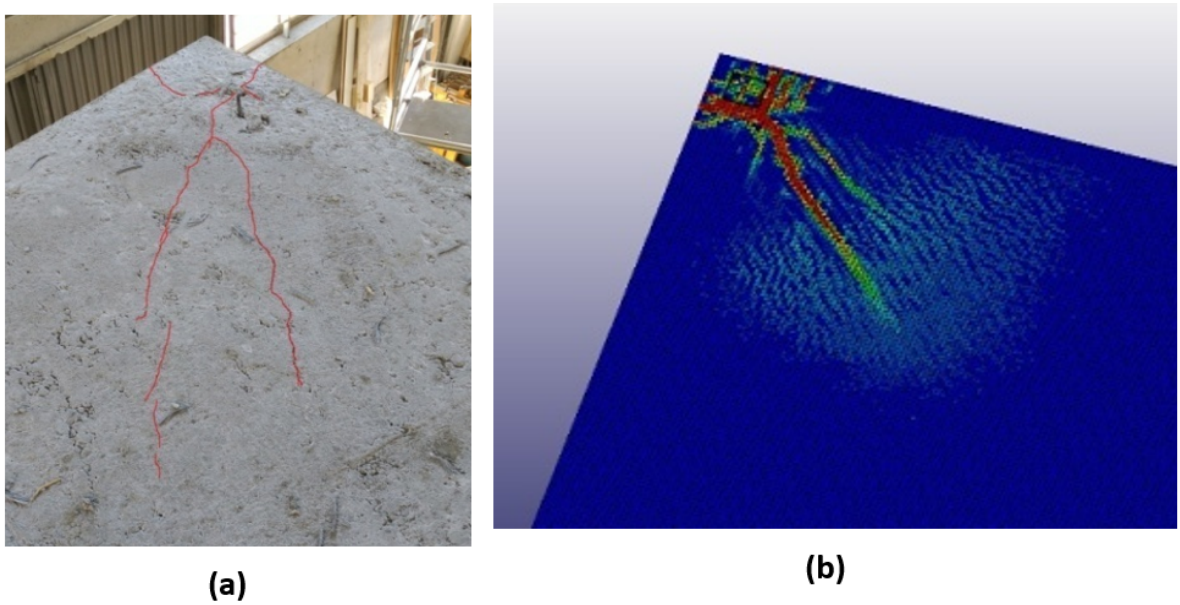

Figure 4.5: Test (a) and FEM (b) top corner crack pattern.

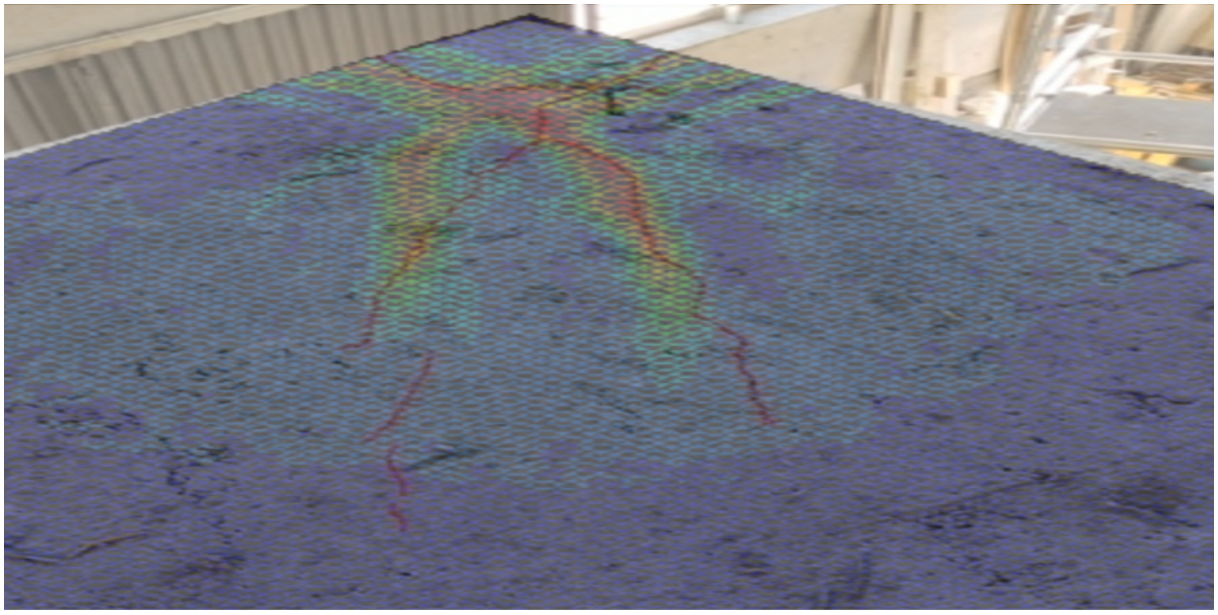

Figure 4.6: Top corner crack pattern FEM and Test superposition

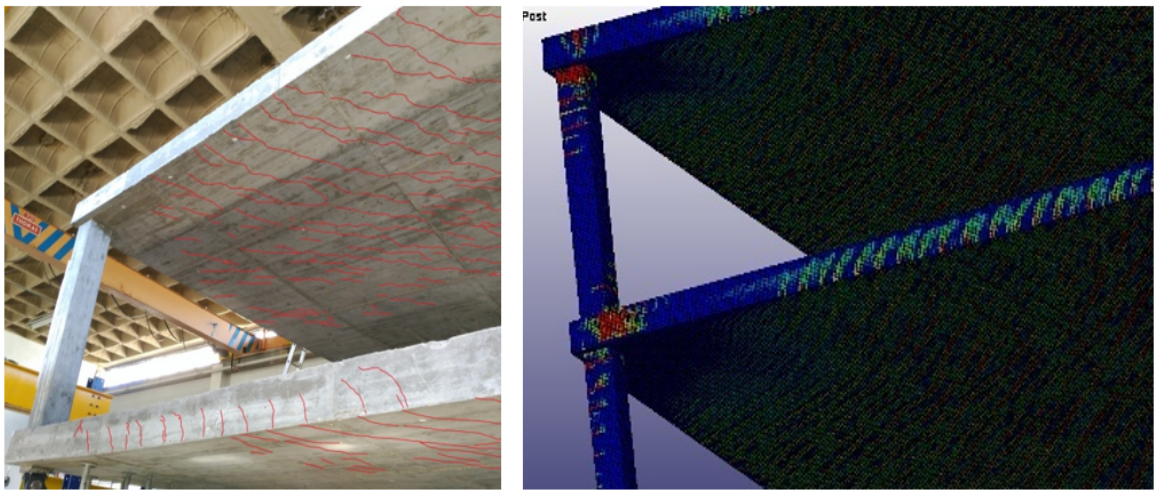

Figure 4.7: Test (a) and FEM (b) top slab crack pattern.

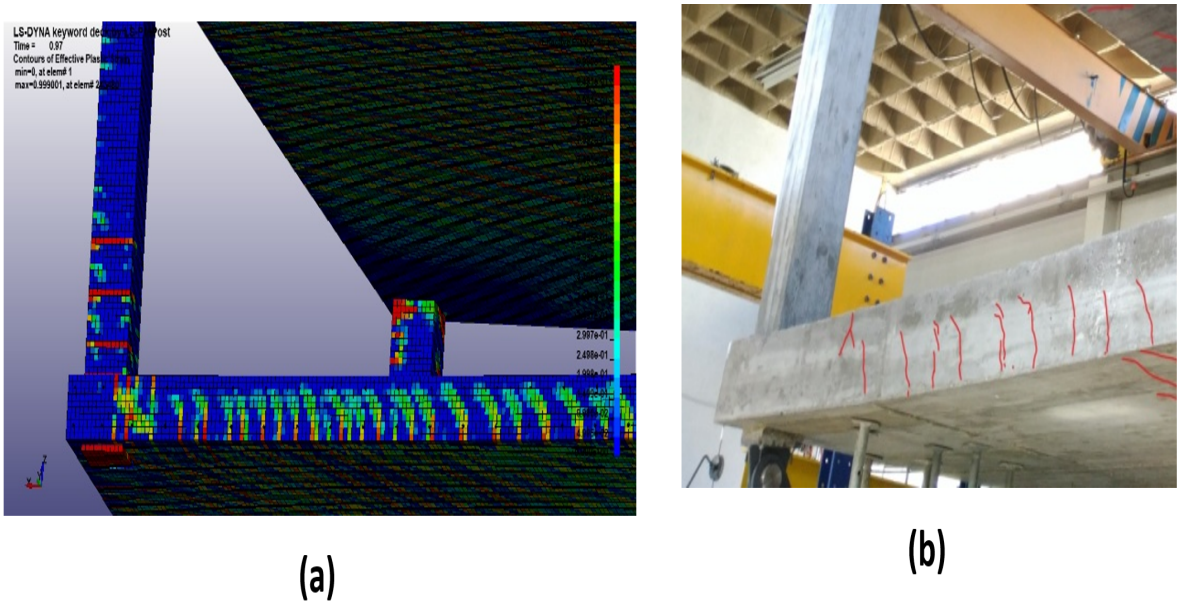

Figure 4.8: Test (a) and FEM (b) slab crack pattern.

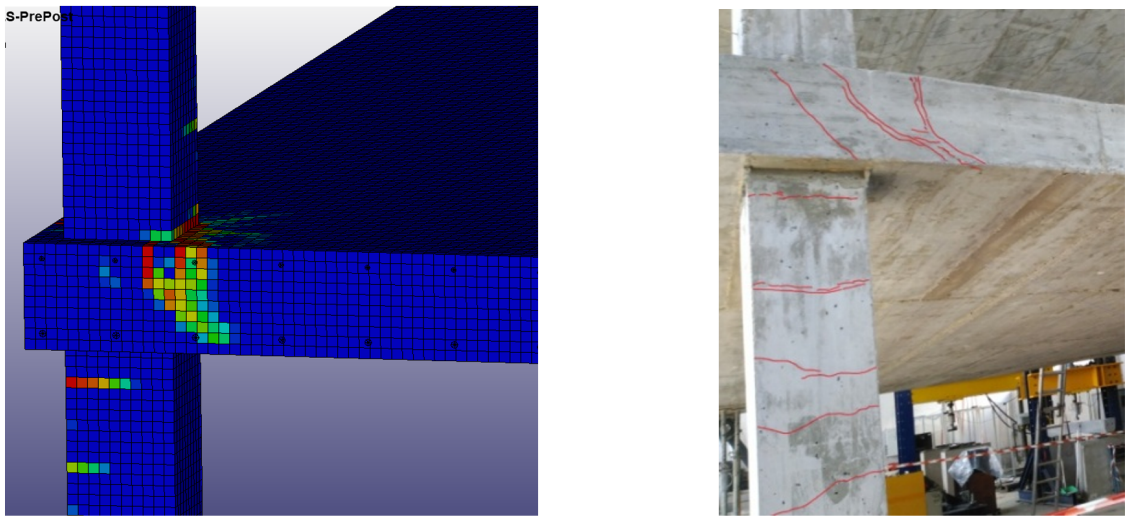

(a) (b)

Figure 4.9: Test (a) and FEM (b) column slab crack pattern.

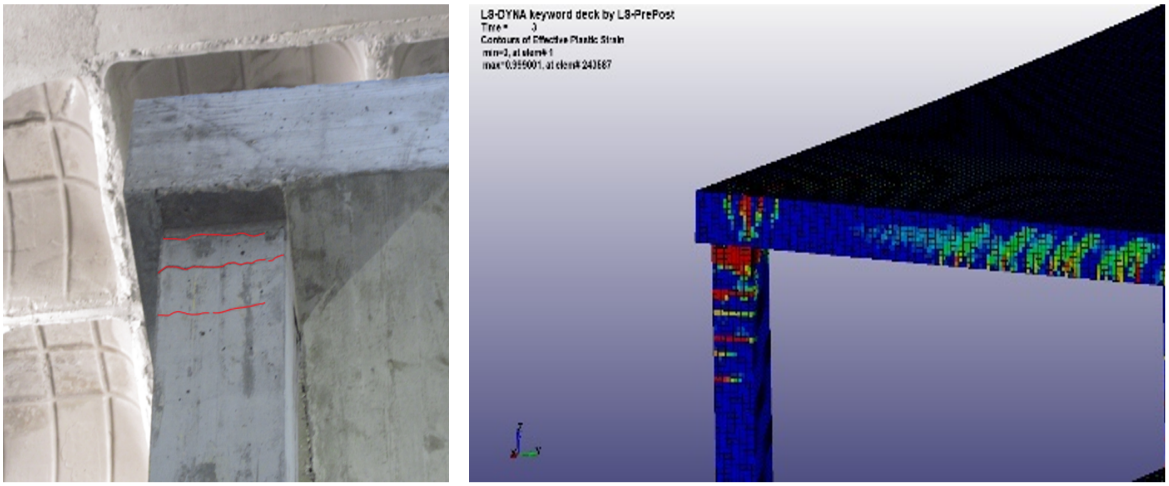

(a) (b)

Figure 4.10: Test (a) and FEM (b) top slab crack pattern.

Figure 4.11 and Figure 4.12 show the cracking patterns predicted by LS-Dyna on the top and bottom surfaces of the top and bottom slab, respectively. The crack pattern in the bottom face of the slabs is consistent with those of a slab working in sagging flexure along an axis with a span length corresponding to the diagonal line perpendicular to the symmetry axis. The diagonal cracks radiating from the supports on the top of the slab are compatible with those on a cantilever spanning parallel to the symmetry axis of the structure. This type of behavior is also illustrated in Melo, 1990 (see Figure 4.13).

Figure 4.5 and figure 4.7 shown a comparison between the cracking pattern predicted by the FEM and the pattern observed in the test, it is evident that both patterns are very similar. Figure 4.8 shows the cracking pattern along the edge of the slabs. These are torsional cracks as their inclination is contrary to the inclination of shear cracks. The connection between the support and the first floor slab shows also such torsional cracks (see Figure 4.9. This is a type of action for which the connection is not designed and failure of this connection could potentially lead to collapse of the structure. This type of cracking pattern, however does not develop at the connection between the column and the top slab because the rotation of the slab is accommodated by more extensive cracking (and possibly yielding of the reinforcement) at the top of the column (see Figure 4.10. The horizontal cracks in the support at the top part of the top column were larger than those observed at the bottom supports. This different behavior is due to the difference in axial force as the compression force in the bottom column is roughly twice the compression in the top columns.
The stresses in the reinforcement are well within the serviceability limits and the width of the flexural cracks was small, around 0.2 mm.

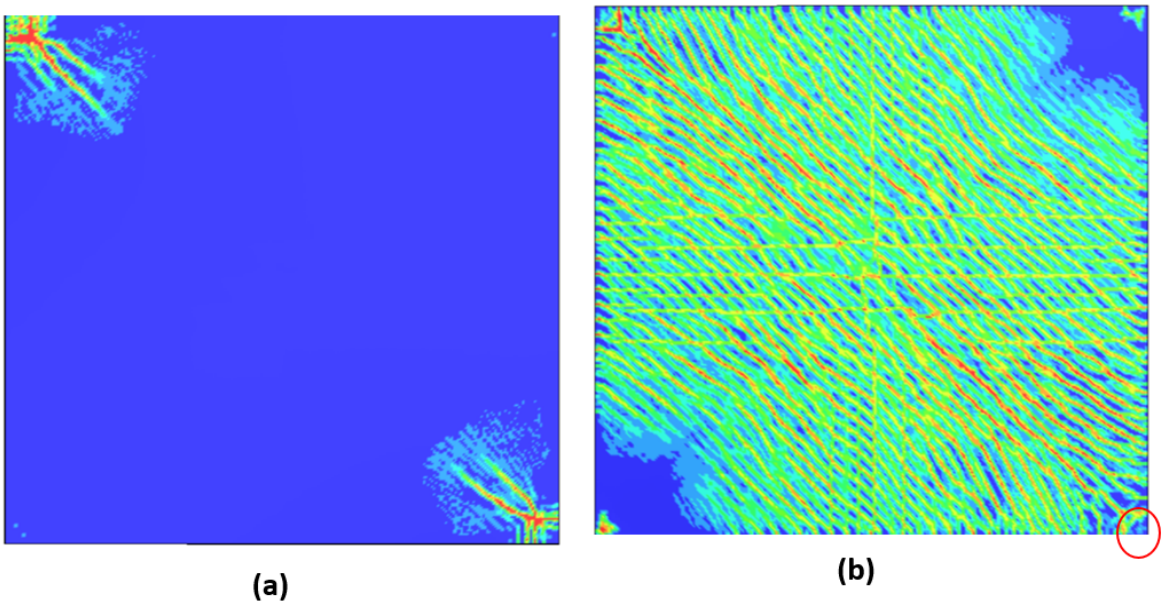

Figure 4.11: FEM crack pattern of Top Slap: Top view (a) and Bottom view (b)

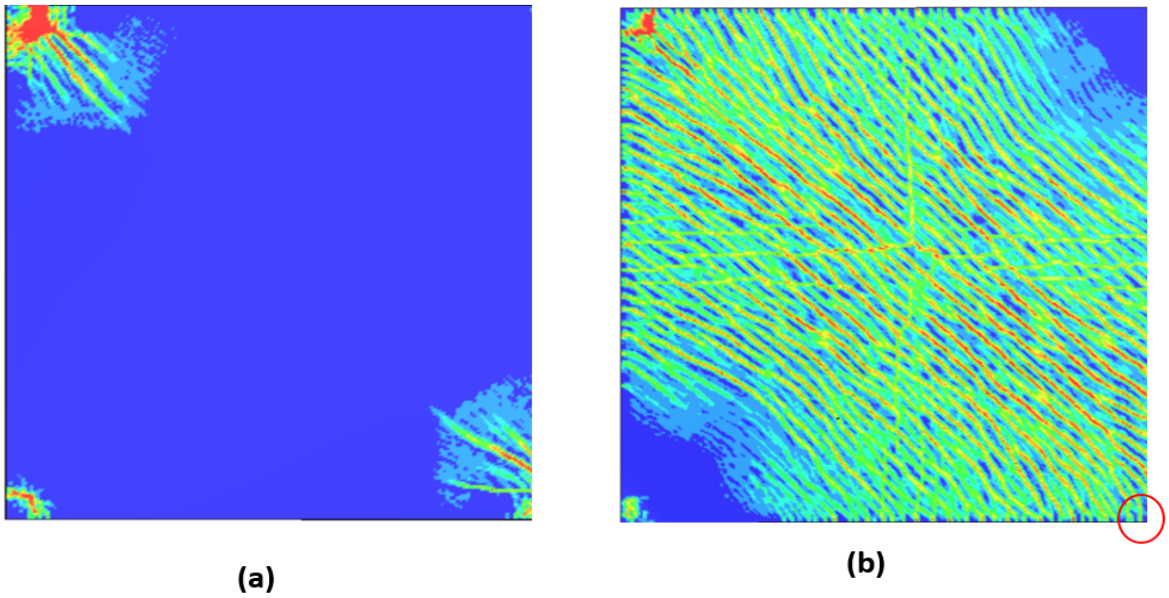

Figure 4.12: FEM crack pattern of Bottom Slap: Top view (a) and Bottom view (b)

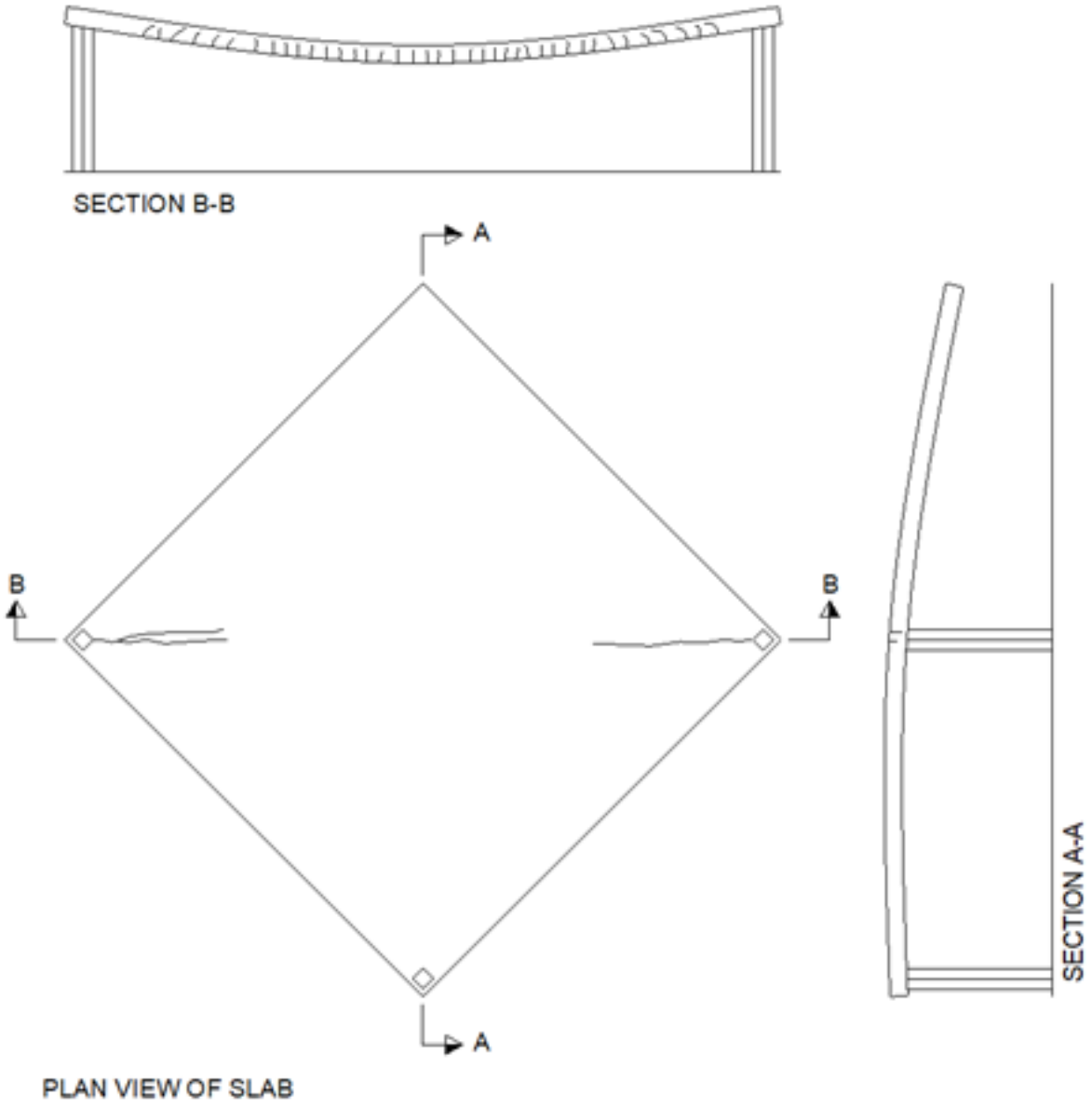

Figure 4.13: Deformation and cracking pattern (conceptual scheme). Cantilever behavior along A-A and simply supported behavior along section B-B. Vertical deflections exaggerated.

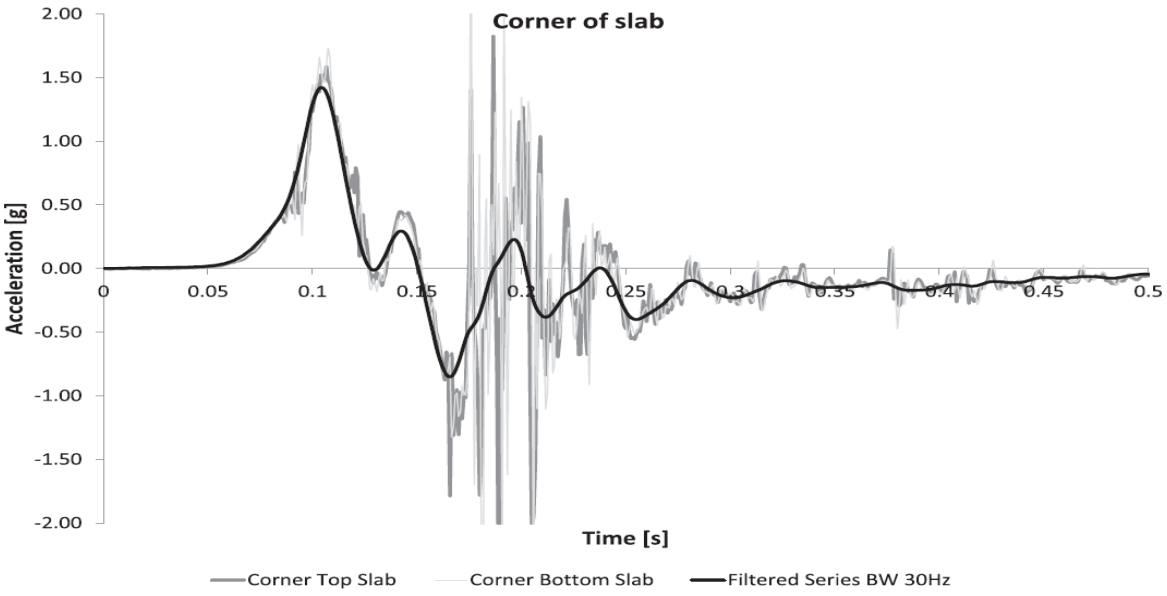

Figure 4.14: Measured accelerations at the corner of the slab (over the removed column)

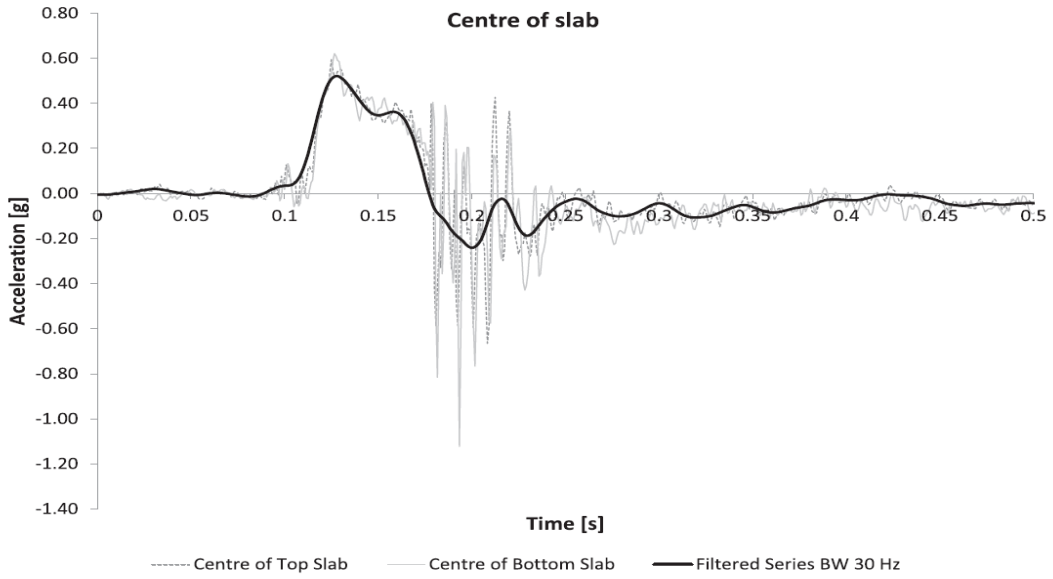

Figure 4.15: Measured accelerations at the center of the slabs)

4.2.2 Two-span concrete frame subjected to successive blast loads

4.2.2.1 Model validation

By using the 3-D laser scan the geometry of the structure was measured before the first blast and after each of the blasts. By subtracting the position of each point after each blast from

their position at the start of the test it is possible to have an estimate of the permanent deflections inflicted on the structure by each blast as well as their cumulative effect. Figure 4.16 shown the three-dimensional representation of the structure obtained by 3D Scanner after Test 3.

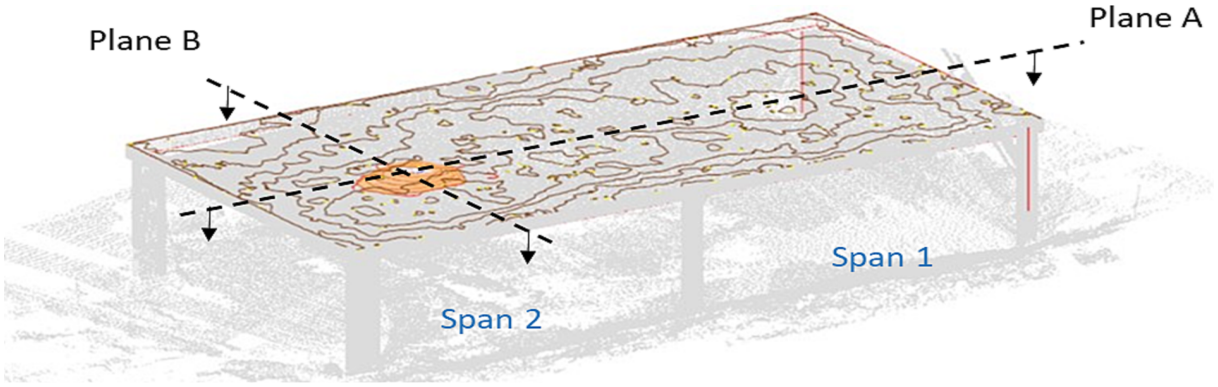

Figure 4.16: Three-dimensional representation of the structure obtained by 3D Scanner after test 3.

Figure 4.17 to Figure 4.19 shows the displacements after each of the three successive tests, taking as a reference the original position (the one prior to test T1). Negative displacement implies downward movement. Test 2 induces an additional downwards permanent load deflection because it contributes to deteriorate the stiffness of the slab for the following reasons:

- Cracking occurs in the supports, and this reduces the embedment of the slab in hogging bending.
- The second explosion] produces an ascending deflection, but once the effect of the overpressure has passed gravity produces a downwards movement which is dynamic.

The self-weight is therefore reapplied on the structure magnified by a Dynamic Load Factor, which contributes to increase the effect of cracking in the slab (reduction of tension stiffening effects). At the end of the second test, the applied load is the same, but the structural stiffness is reduced resulting in a larger deflection. The values of the permanent deflections are small, less than 20 mm for the two first blasts and only 35 mm after the third blast which does inflict local damage on the structure. Note that the deflection at the perforation of the slab corresponds to the bent reinforcement which is captured by the laser-scanner. The results show that the structural solution adopted for the floor has a high degree of robustness and could withstand this range of explosive action with only local damage, without any special measures.

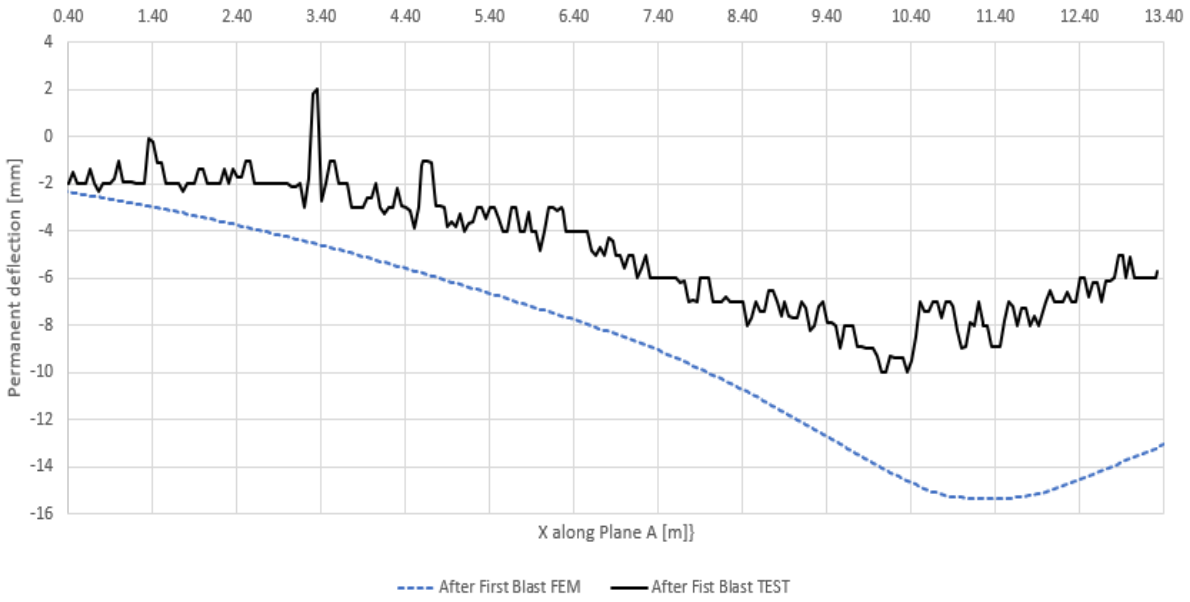

Figure 4.17: Comparison of experimental and FEM results for permanent displacement history along the longitudinal axis of the structure (Plane A) Test 1.

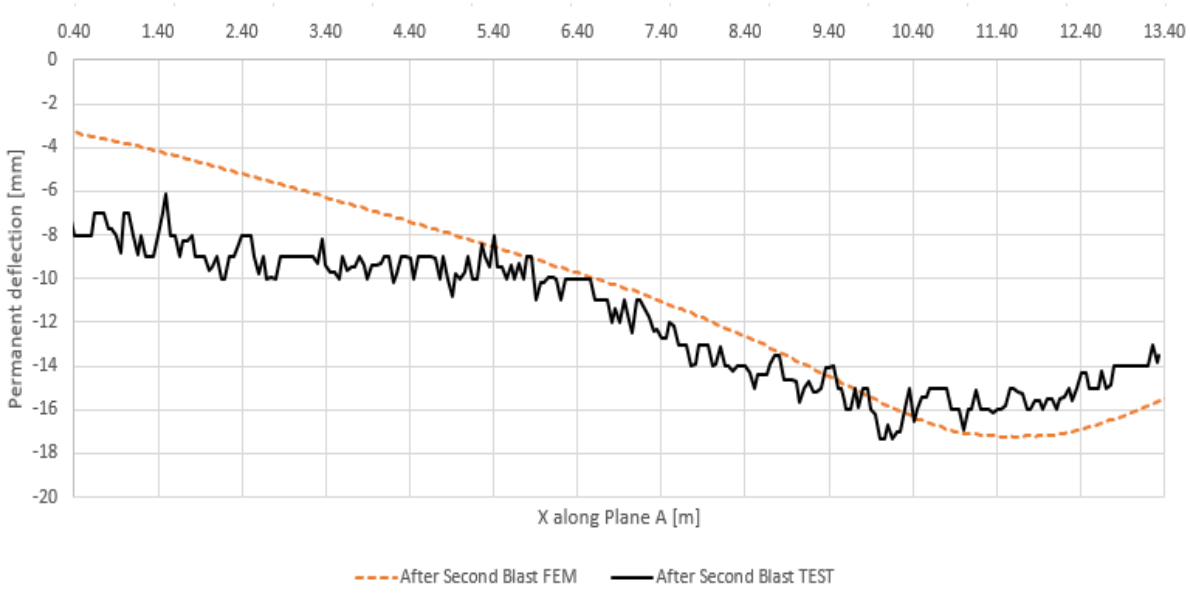

Figure 4.18: Comparison of experimental and FEM results for permanent displacement history along the longitudinal axis of the structure (Plane A) Test 2

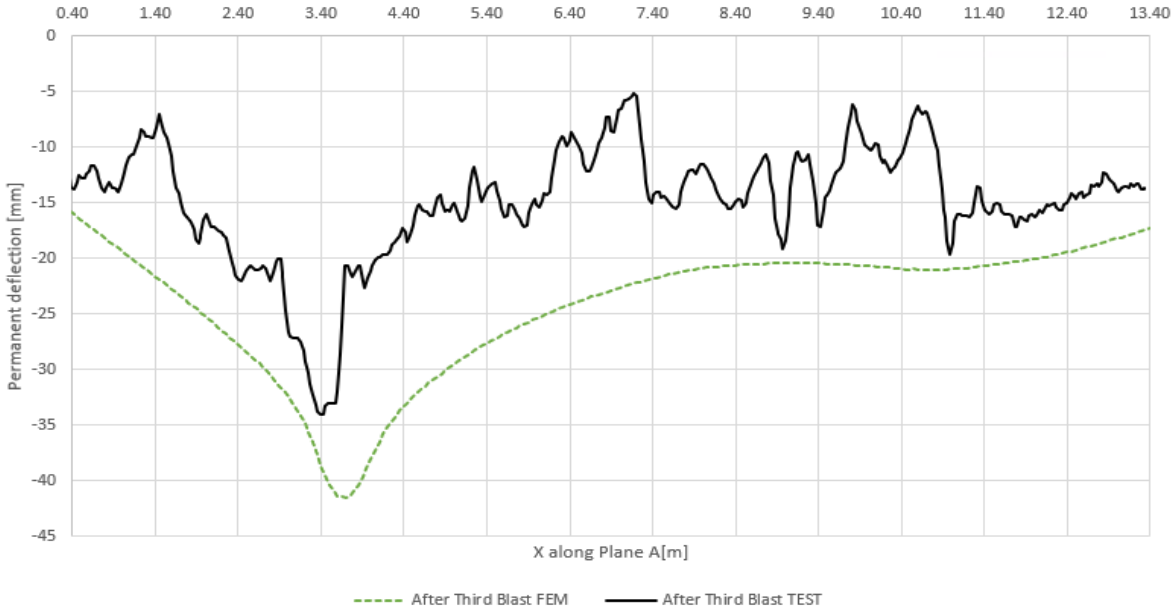

Figure 4.19: Comparison of experimental and FEM results for permanent displacement history along the longitudinal axis of the structure (Plane A) Test 3.

The FEM nodal displacements of the LS-DYNA simulation exhibited approximately the same trend as the experimental values. The maximum deflection is 15 mm after first blast, 17 mm after second blast and 42 mm after the third blast. Figure 4.20 to 4.22 shown comparisons between deflections measured by laserscan and the numerical simulations. The shapes and values obtained by the simulation are reasonably close to those of the tests.

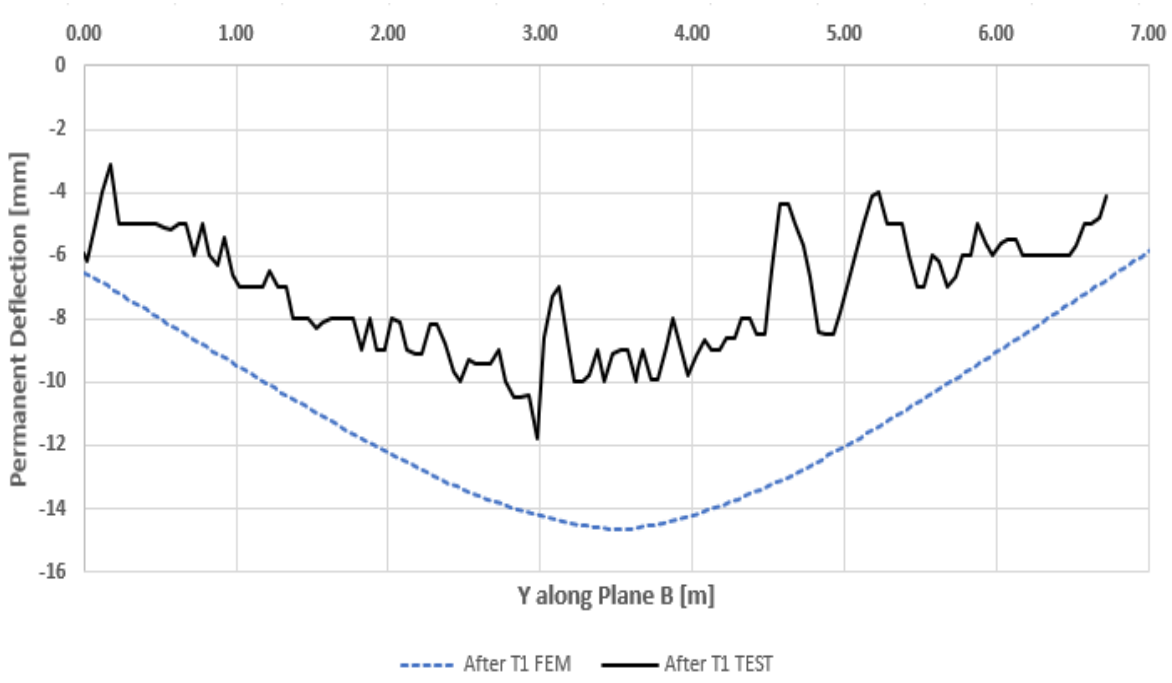

Figure 4.20: Comparison of experimental and FEM results for permanent displacement history along the transversal axis of the structure at Plane B. Test 1.

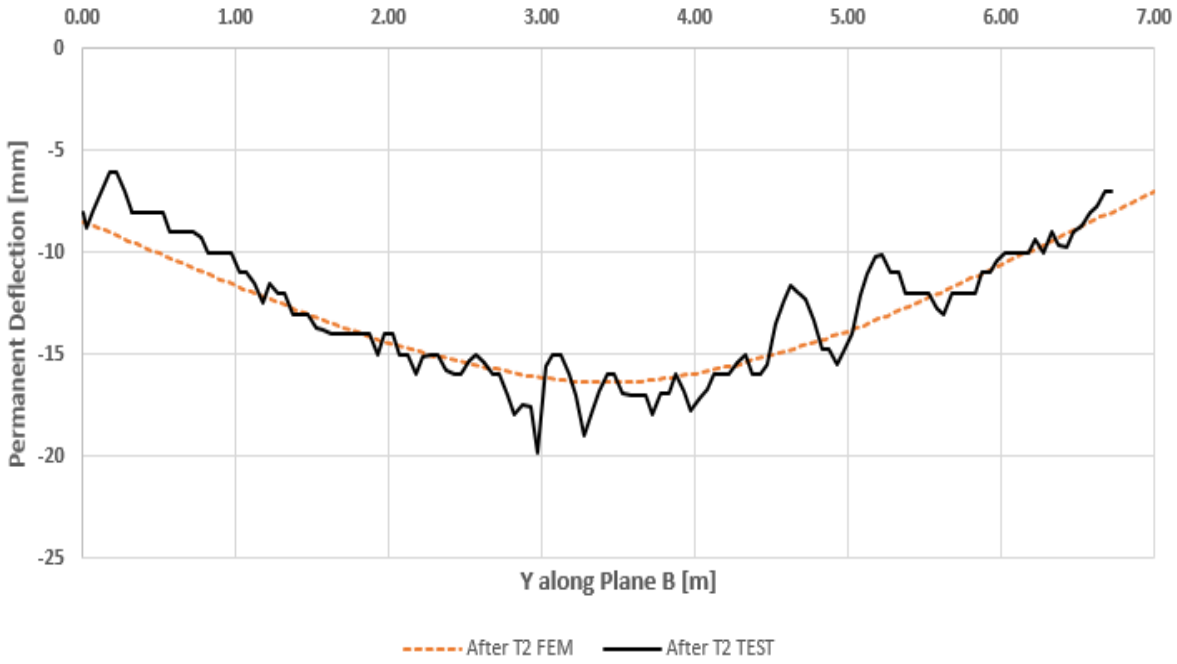

Figure 4.21: Comparison of experimental and FEM results for permanent displacement history along the transversal axis of the structure at Plane B. Test 2.

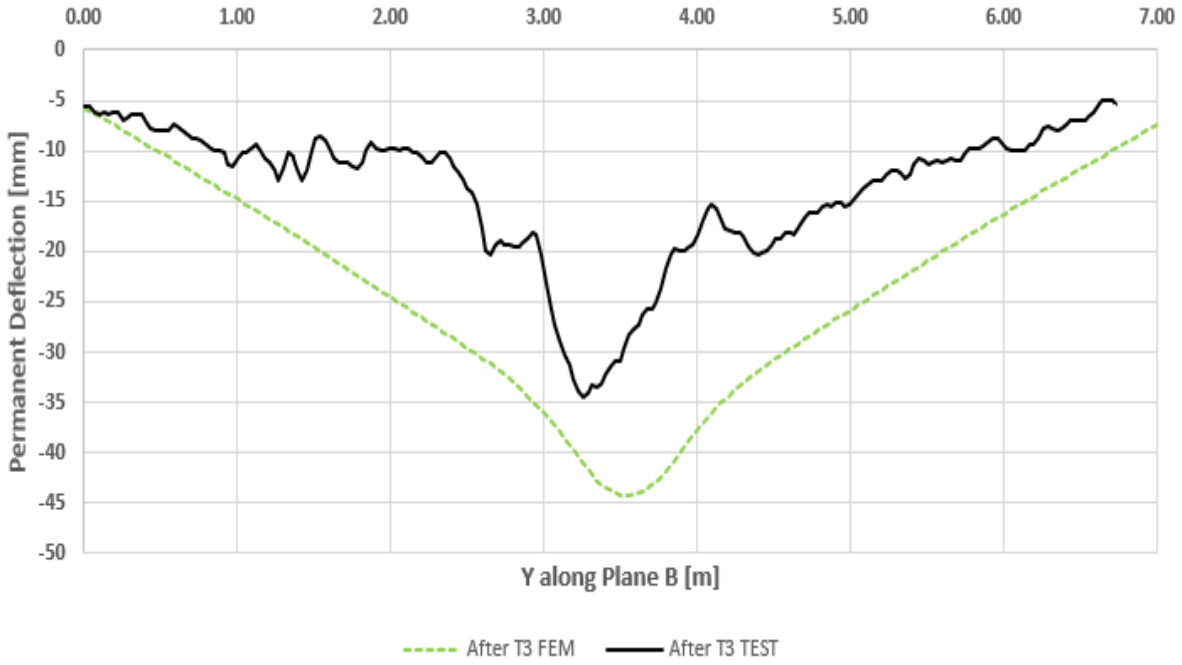

Figure 4.22: Comparison of experimental and FEM results for permanent displacement history along the transversal axis of the structure at Plane B. Test 3.

Experimental acceleration records are used to check the goodness of fit of the model. In Figure 4.23 the records obtained by the model are plotted together with the experimental ones at sensor position A1. It can be seen that although the shape of the signals is not the identical, the maximum and minimum acceleration values are approximate. The experimental acceleration ranges from -90 g to 84 g while in the model it ranges from -85 g to 71 g for T1 test. And in the T2 test, the experimental acceleration range is - 108 to 182 while the model gives accelerations between -156 and 137 g.

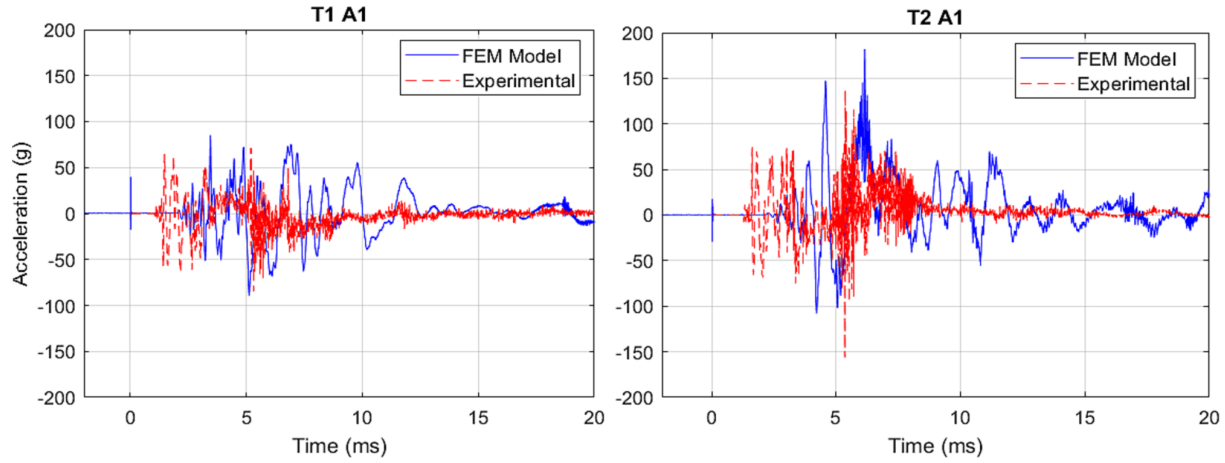

Figure 4.23: Accelerations obtained experimentally and by modelling sensor S1 tests T1 and T2.

In the first two scenarios, despite the non-negligible mass of the explosive used, damage to the structure even ignoring the blast loads in the design, is quite small. Figure 4.24 shows images of the damage after each of the tests. Damage is limited to the appearance of flexural cracking in the bottom face of the slab after the first blast and horizontal cracking in the supports near the connection to the slab after the second blast load.

Figure 4.24: Damage to concrete after each test.

When for the third test the 20 kg TNT equivalent load is placed only 50 cm away from the slab surface, damage does occur, but it is local and consists of a perfectly circular punching failure. Figure 4.25shows several images of the structure after Test number 3. When for the third test the 20 kg TNT equivalent load is placed only 50 cm away from the slab surface, damage does occur, but it is local and consists of a perfectly circular punching failure. Figure 4.25 shows several images of the structure after Test number 3.

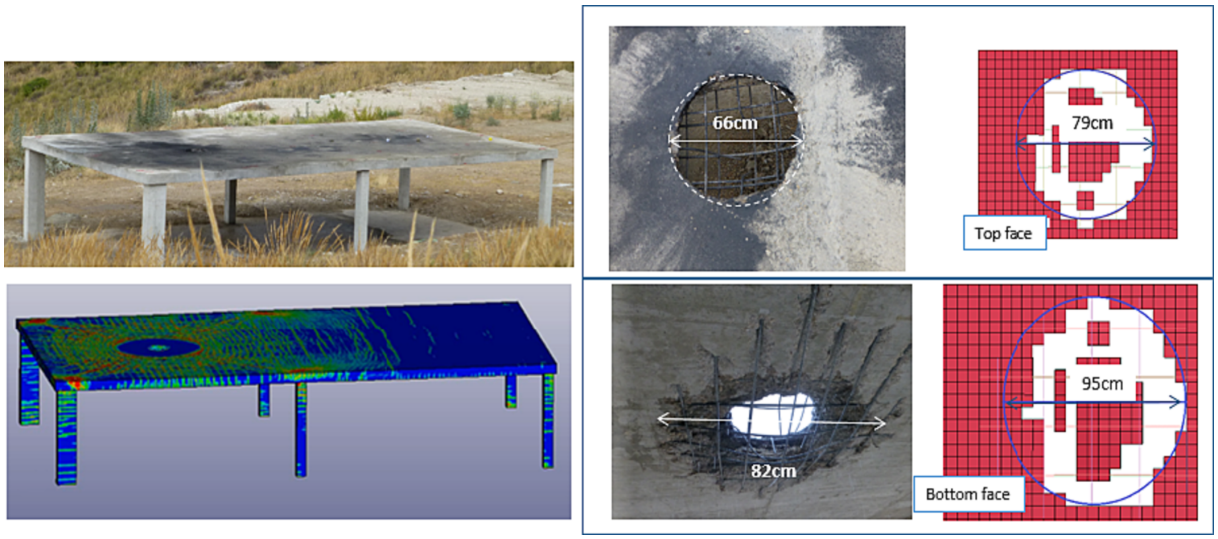

Figure 4.25: Experimental and FEM structure after T3 Test.

The crater generated in the slab is about 66 cm of diameter on top face. The bottom face shows a spalling surface of approximately 82 cm in diameter. The results of the FEM model

show a cracking pattern on top face of approximately 79 cm of diameter while the bottom face presented a cross-shaped spalling with a maximum length of 95 cm. The FEM provides a reasonable order of magnitude, usable in practice, without need for further adjustments.

Chapter 5

Numerical Investigation

5.1 Introduction

In this section the analysis of membrane forces is made using different tools. First a simple Strut and Tie analysis is made which provides an idea of the orientation of the membrane forces. This is already a useful tool to assess capacity. Then some considerations based in linear elastic analysis are made. These considerations are useful when critically reviewing the results of nonlinear FEM, which can lead to significant differences depending on the type of analysis made and even on the software used. Robustness analysis and minimum reinforcement methods such as that proposed in EN 1991-7 Standard, 2006 rely for the resistance of a structure after a column removal on the formation of an alternate load path in which the slab deforms enough vertically to generate membrane forces whose vertical component can balance the gravitational loads after the support's collapse. As it cannot be guaranteed that the horizontal force generated by tension membrane forces can be resisted by the surviving columns, a self-equilibrating strut & tie scheme contained within the plane of the slabs must be found to guarantee equilibrium. It will be shown that this is not always possible when more than one support collapses. Following, possible strut & tie models corresponding to the two structures which have been tested are examined.

5.2 Two-story concrete slab with corner column removal

5.2.1 Strut and tie model

Figure 5.1 shows a possible strut and tie model to balance the gravitational forces after the loss of the corner support in the two-story structure. At first, the structure will attempt to resist the gravitational forces by flexure. On the top face of the slab, this will generate a cracking pattern in the direction of the diagonal connecting the two supports adjacent to the

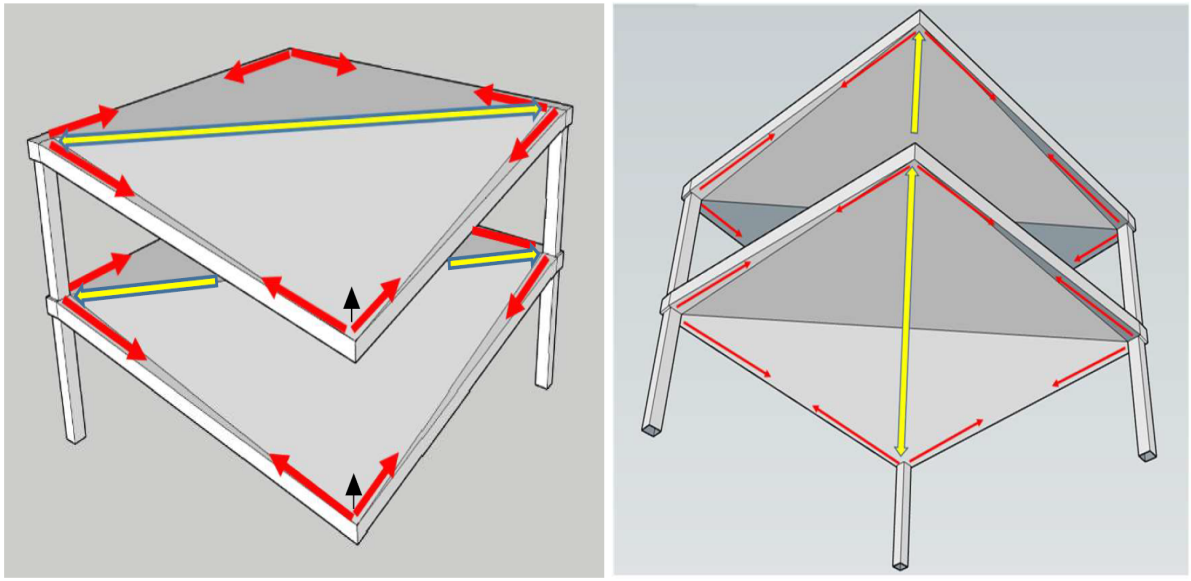

Figure 5.1: Possible Strut and Tie model to resist the gravitational forces of the two-story slab after removal of the corner support (drafted using Sketchup)

collapsed column. There will be cantilevering action as the slab tries to resist as embedded along that diagonal. On the bottom face, cracks will form in the direction perpendicular to this diagonal as the slab tries to resist through sagging bending with a span equal to the diagonal length. This cracking pattern of the slab will determine the orientation of the struts on each face of the slab. They will be parallel to the bending cracks that have previously formed. Both the upper and lower reinforcements could be mobilized at the nodes. Using this model, a very simple analysis can be performed to ascertain what the maximum capacity of the slab without the corner column would be. Assuming that the slab is fully loaded up to its ultimate load before column failure, this would lead to a distributed force of 21.3 kN/m^2 as shown in Equation 5.1. In this equation the support reaction of the support to be demolished is also shown.

$$q_u \frac{L^2}{8} = m_u^- \rightarrow q_u = 8\frac{116}{6.6^2} = 21.3kN/m^2 \tag{5.1}$$

$$R_u = q_u \frac{L^2}{4} = 21.3\frac{6.6^2}{4} = 232kN \tag{5.2}$$

5.2.1.1 Linear Finite Element Analysis

Figure 5.2 shows the linear elastic moments due to a total load of 12 kN/m^2, equal to twice the dead load of the structure. The distribution of negative bending moments along the diagonal that joints the two supports adjacent the one collapsed, concentrates negative bending at the edges near the support, which is not evident, while positive bending occurs in the perpendicular direction. As mentioned above, the negative bending capacity of the slab is 77 kNm/m while the positive bending of the central strip (where bending moments are

highest after column collapse) is 116 kNm/m. It is clear that without membrane forces some redistribution of forces is necessary to resist the forces.
Membrane forces can be simulated using linear elastic analysis by providing the structure with a curved geometry, resembling the one expected to occur. One possible shape to simulate this curvature is given in Equation 5.3. The deformed shape is assumed to follow a sine function along the line connecting the two supports adjacent to the collapsed one (y') and a second degree law along the perpendicular axis (x').

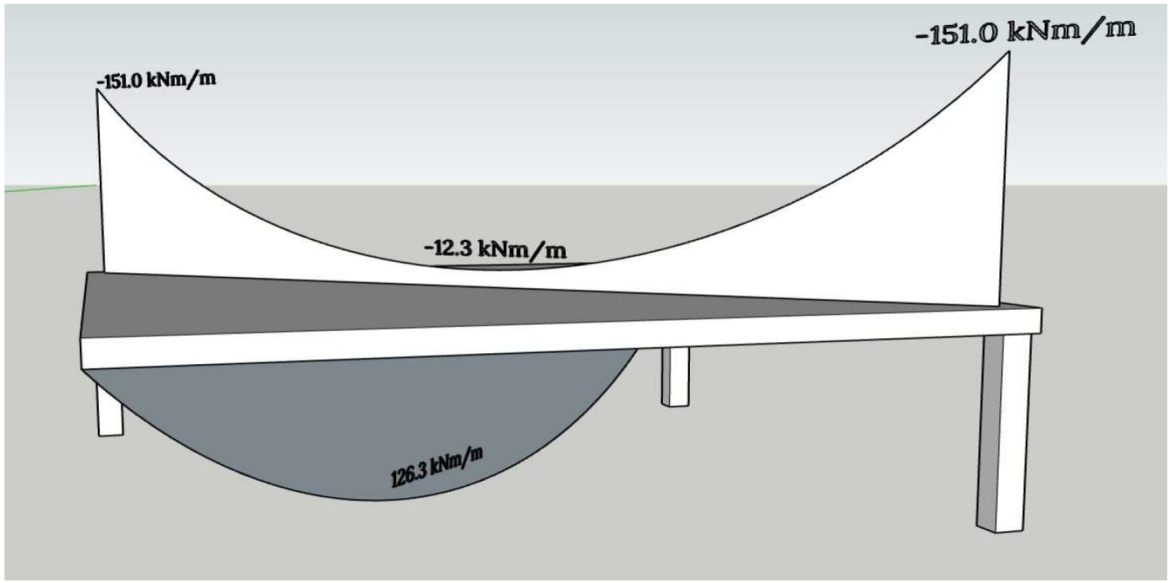

Figure 5.2: Linear elastic moments along diagonals (drafted using Sketchup)

$$z = sin\left(\frac{\pi}{L\sqrt{2}}\left(\frac{L}{\sqrt{2}} - y^{'}\right)\right)\left(\frac{\delta_2 - 2\delta_1}{L^2}x^{'2} + \frac{4\delta_1 - \delta_2}{L}x^{'}\right) \tag{5.3}$$

Where:

L	is the span of the slab (6.6m).
x', y'	are the coordinates along the main diagonals.
δ_1	is the displacement at the center of the slab
δ_2	is the displacement at the axis of the collapsed support

From linear elastic finite element analysis, it was found that δ_2 =2.54 δ_1. It is interesting to see how membrane action develops using linear elastic calculations when the slab is deformed according to the above equations.
A pattern of principal membrane forces which are fully compatible with the strut & tie model shown above develops, as can be seen in Figure 5.3. The principal membrane forces nI shown on the left clearly show the tension forces in the perimetral ties while the principal membrane forces nII correspond to the diagonal struts necessary to equilibrate the change of direction in

the forces of the ties at the corners.

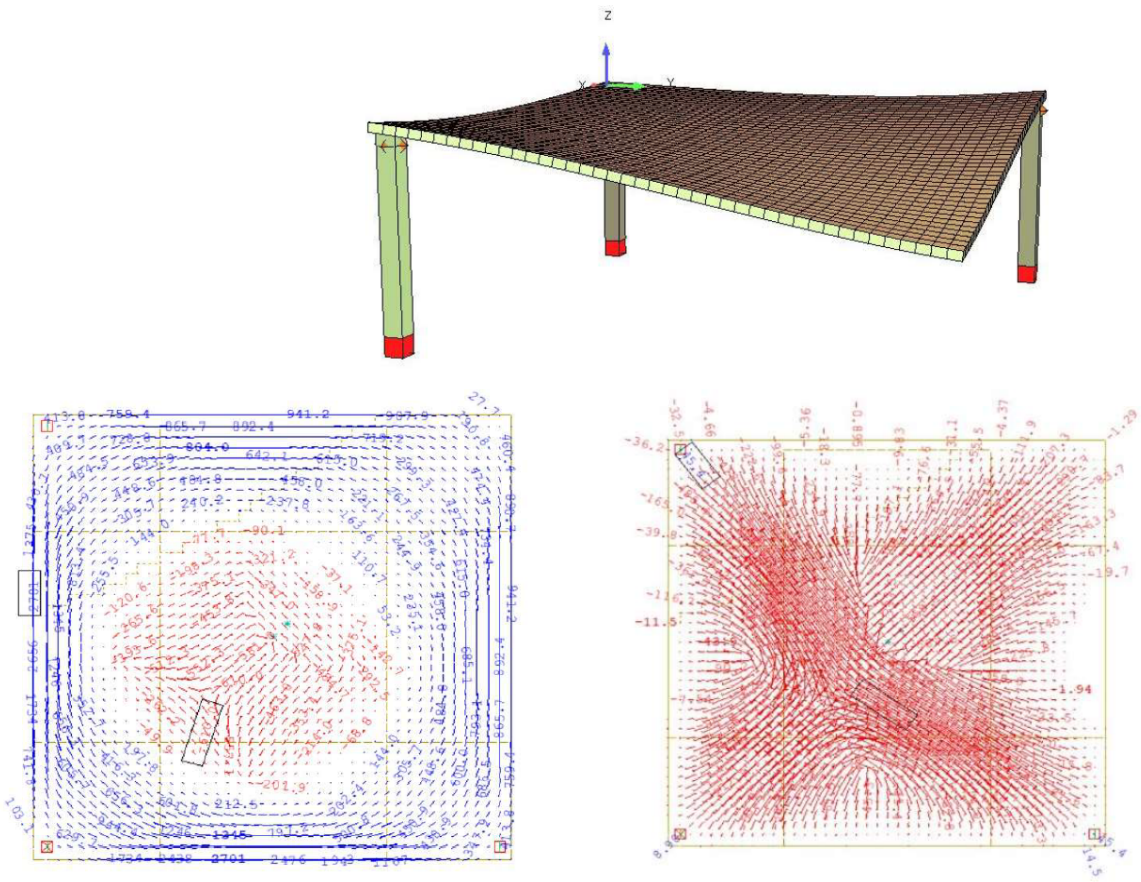

Figure 5.3: Membrane forces generated in the slab with a load of 12 kN/m^2 and a maximum displacement of 1000 mm. Top: model geometry. Bottom left: principal membrane forces nI. Bottom right: principal membrane forces nII (results form a linear elastic SOFISTIK model)

By assuming different maximum deflections, the variation in the bending and axial forces in the diagonals can be determined using linear elastic analysis. Figure 5.3 shows the bending moments and axial forces along the two principal diagonals as a function of the maximum vertical displacement of the structure. These results are obtained from linear elastic analysis of the deformed structures. The figure shows the appearance of significant membrane forces which, however, have only a small influence on the bending moment laws. This shows the much more complex behavior of 2-D elements with respect to unidirectional elements with external restraint. The maximum negative bending moment along the diagonal joining the two supports adjacent to the collapsed one exceeds the sectional capacity. However the section is ductile (it only has a reinforcement of ϕ12@0.20 and with a little redistribution (in a width close to only 2.00 meters) the section can resist the bending forces with the accompanying tensile membrane forces. Although this figure is drafted for a force of 12 kN/m^2, since the model is linear, it can be used to predict the forces due to any other load. As will be shown

later, finite element analysis predicts the collapse of the structure for a load of 15.25 kN/m^2 which seems to be in contradiction of the strut and tie analysis of the previous paragraph as well as with the results shown here. This does not seem to be because of the bending forces since further re distributions would certainly be possible.
An interesting feature, which can be seen from Figure 5.4, the progressive development of positive bending forces (rotating along the y' axis) in the central part of the structure is due to the arching curvature of the compressed center in which the compressive strut parallel to the x' axis generates an upwards component which helps balance gravitational forces.

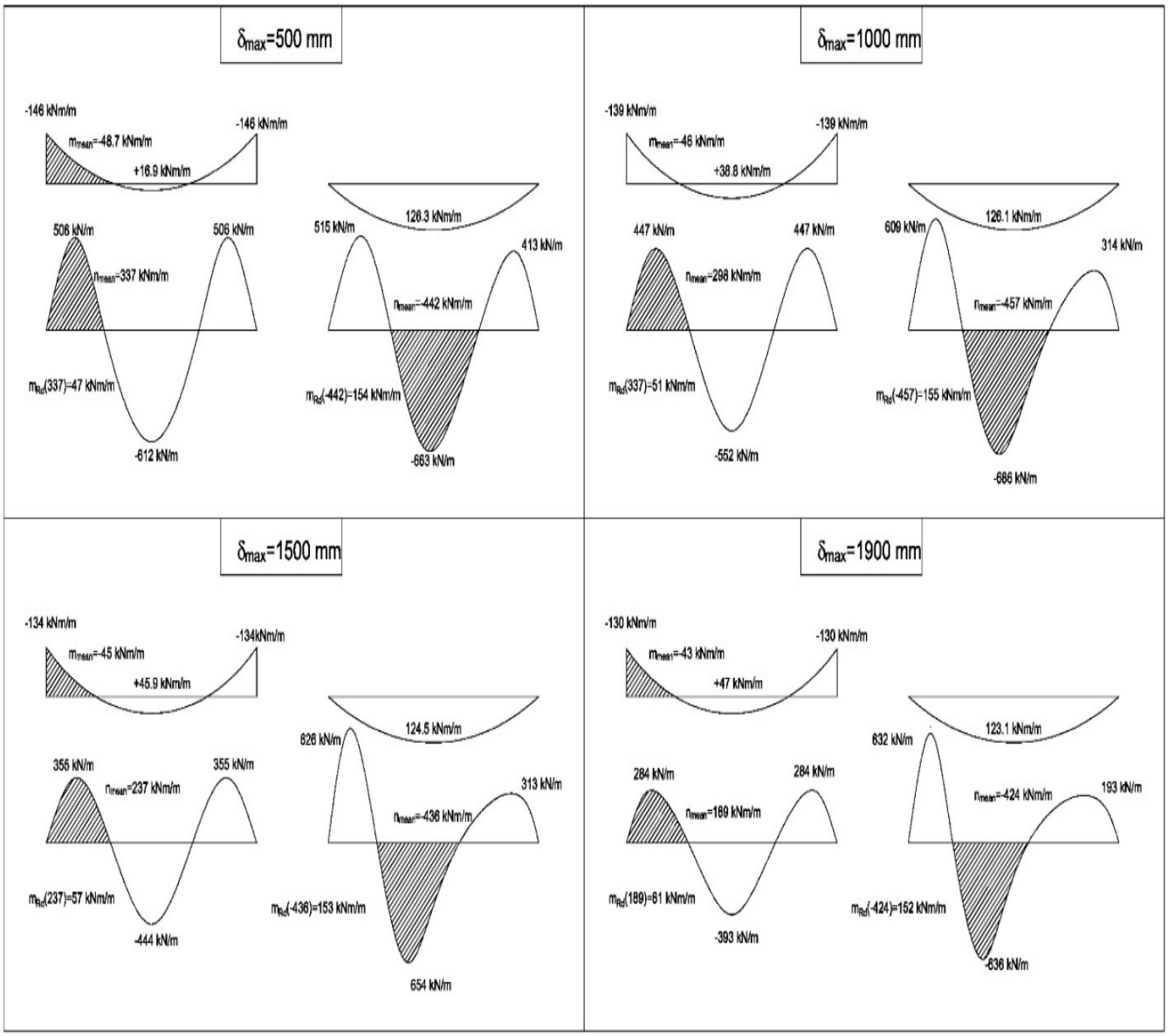

Figure 5.4: Variation of forces and bearing resistance as a function of the maximum deflection and generation of membrane forces (linear elastic analysis of deformed structure)

5.2.2 Linear finite Element Analysis

5.3 Two-span concrete slab with intermediate column removal

5.3.1 Strut and tie model

For the two-span structure, a balanced strut and tie model can also be found for the equilibrium of the structure when the first support collapses as shown in Figure 5.5. Note that when the strut of the bottom face crosses the rupture line, an upwards force is generated (see Figure 5.6). However there is no possible strut and tie model that can balance the structure when the second central support is removed that does not involve the bending and shear resistance of the supports, which in this case is insufficient to avoid collapse. The reason for this is in the shape of the rupture line (or the direction of the curvature). The compression force cannot cross this line without producing a downwards thrust which undoes the effect of the upwards vertical component of the tension reinforcement (see Figure 5.7 and Figure 5.8). This explains why the structure failed when the second support was removed.

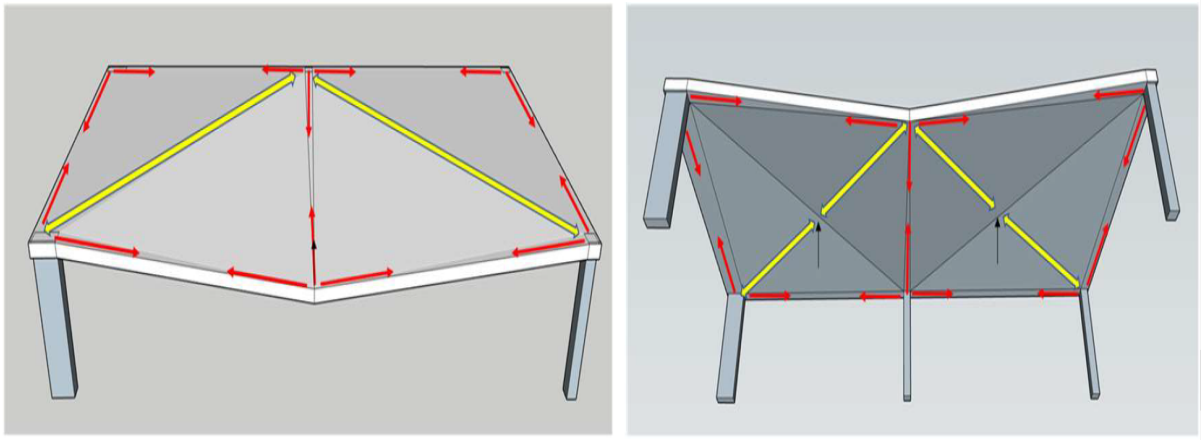

Figure 5.5: Possible Strut & Tie model to resist the gravitational forces of the two-span slab after removal of the corner support (drafted using Sketchup)

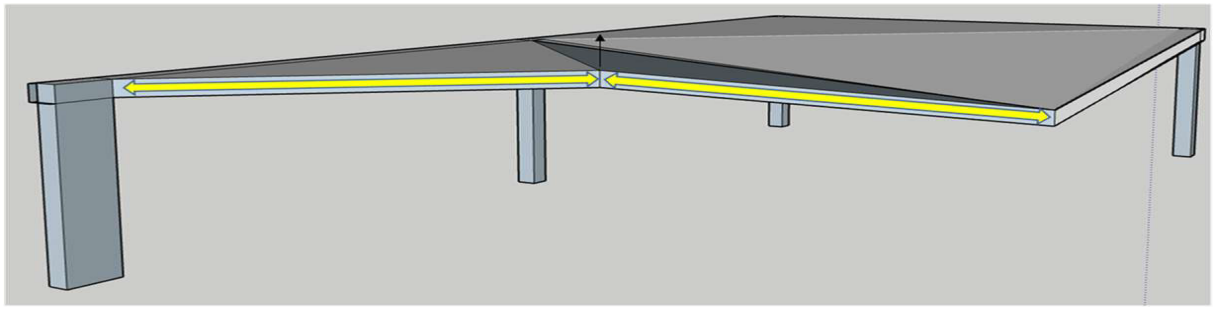

Figure 5.6: The strut crossing the rupture line generates an upwards thrust which helps to resist gravitational loads (drafted using Sketchup)

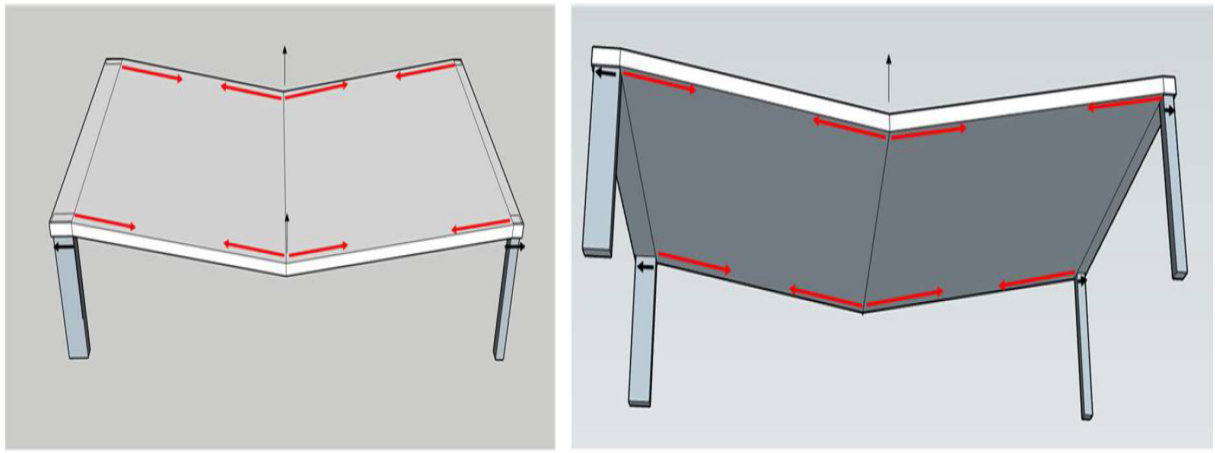

Figure 5.7: Strut and tie model to balance the structure when two supports are removed. The model involved the shear and bending resistance of the supports (drafted using Sketchup)

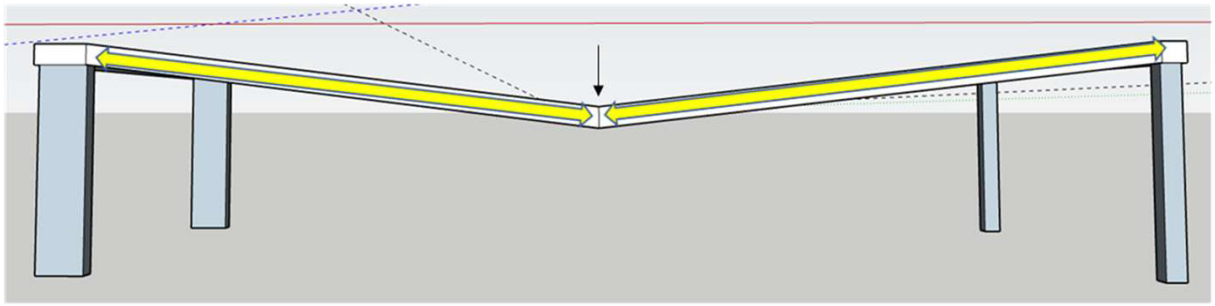

Figure 5.8: A strut crossing the rupture line would generate a downwards resultant undoing the effect of the tension reinforcement (drafted using Sketchup)

Chapter 6

Detailed analysis of the resistance mechanisms for robustness of structures

6.1 Introduction

As explained in the Introduction, the objective of this thesis is to determine the importance of the membrane effect when a column is lost under real conditions. Most of the studies, both experimental and analytical (see, for instance, Gouverneur, 2014) focus on uniaxial behavior, where the membrane action is induced by a horizontal restraint. This does not correspond to the actual functioning of structures in which the membrane forces form a self-equilibrating system of actions where both tensile and compressive forces, which cancel each other as a sum are generated. In the typical case of loss of a central support, the bending moments across a section parallel to a side along the section of the lost column are resisted by means of two mechanisms. In the central zone, where the deflections are higher, tensile membrane forces are generated, and these forces, multiplied by the deflection, generate a balancing bending moment. In this area the contribution to resistance of bending is small due to the effect of the tensile forces. On the sides, close to the edge columns, compression membrane forces are generated, and these provide negative bending moments that are smaller than those generated in the central part because deflections are smaller. However, the main effect of the compression force in this area is to increase the negative bending capacity of the slab in the zone of the edge columns (column strip). So, the side areas function as expected in negative bending with a capacity enhanced by the membrane effect of the compression forces and the contribution of compression to flexural capacity, while in the center the unexpected positive bending moment caused by the column collapse is resisted mainly by positive-moment membrane action. The following is a study of the case of a central support with increasing load, in which the relative importance of membrane action is determined as a function of the applied load.

6.2 Description of the structure

The structure considered is a two-span solid slab supported of isolated columns (25x25 cm2) with 6.6 m spans. The shear and bending stiffness of the columns is represented by springs. Their stiffness is the linear stiffness divided by a factor of 2 to account for cracking. As can be seen in Figure 6.1 and Figure 6.2, the central support is missing.

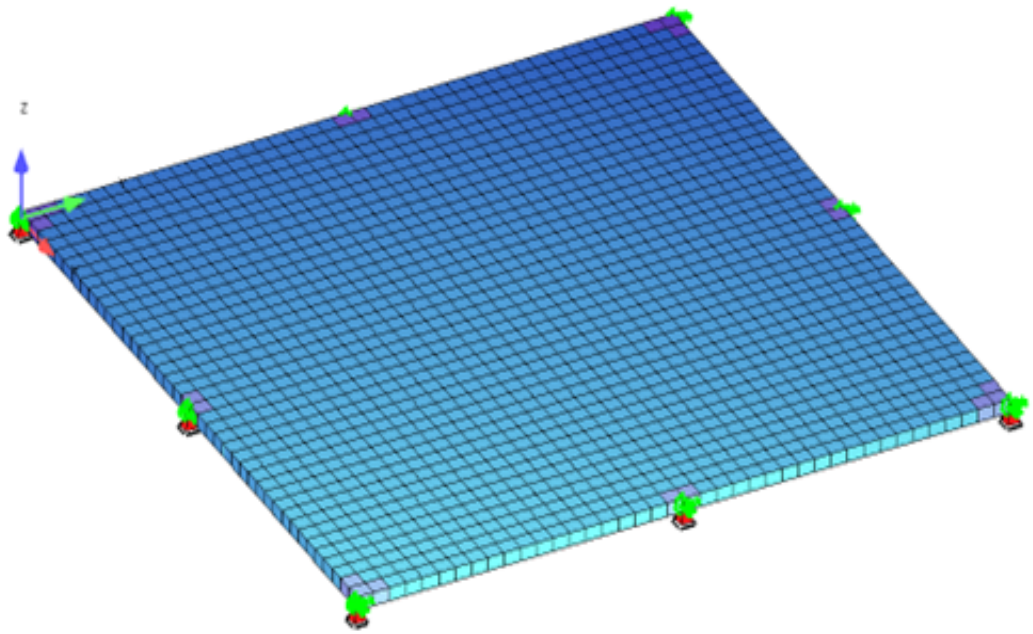

Figure 6.1: View of the model from above

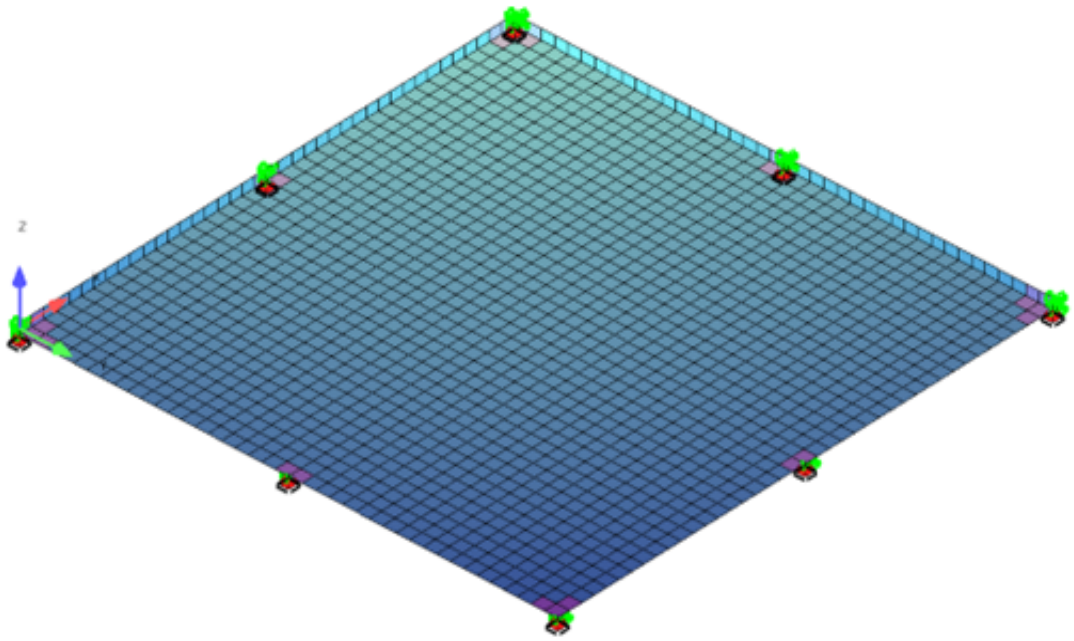

Figure 6.2: View of the model from below

Another feature of the model is that due to the simplifications adopted, the column support is modeled as a point support. The behavior of the material around the support is assumed to be linear elastic to avoid unrealistic local failure in the model. The stiffness considered for these elastic elements is the gross stiffness divided by 3 to account for cracking. In the figure, the linear elements appear in a slightly different color. Calculations were made for the following load levels:

- Self-weight of the slab, equivalent to 6.25 kN/m^2
- 1.25 times the self-weight (7.81 kN/m^2)
- 1.5 times the self-weight (11.5 kN/m^2) this step was used for comparison purposes with a parallel model
- 2.00 times the self-weight (12.5 kN/m^2)

These load levels are used because they seem realistic for actual applications.

Regarding the definition of reinforcement, a base mesh of 12 mm in diameter is placed every 20 cm on both sides of the slab (top and bottom) and in both directions (X and Y). In addition, a 16 mm every 20 cm reinforcement with a length of 1/3 of the span is placed at the top of the slab in the column strips on the central and edge supports. Finally an additional reinforcement of 12 in diameter every 20 cm is placed at the bottom face of the slab in the positive bending zones of the column strips. This reinforcement corresponds to a conventional

design of the structure for typical loads (self-weight, 1.5 kN/m^2 of superimposed dead load and 3 kN/m^2 of live load). The ultimate bending moment without axial force for negative bending is 170 kNm, as can be seen in Figure 6.3

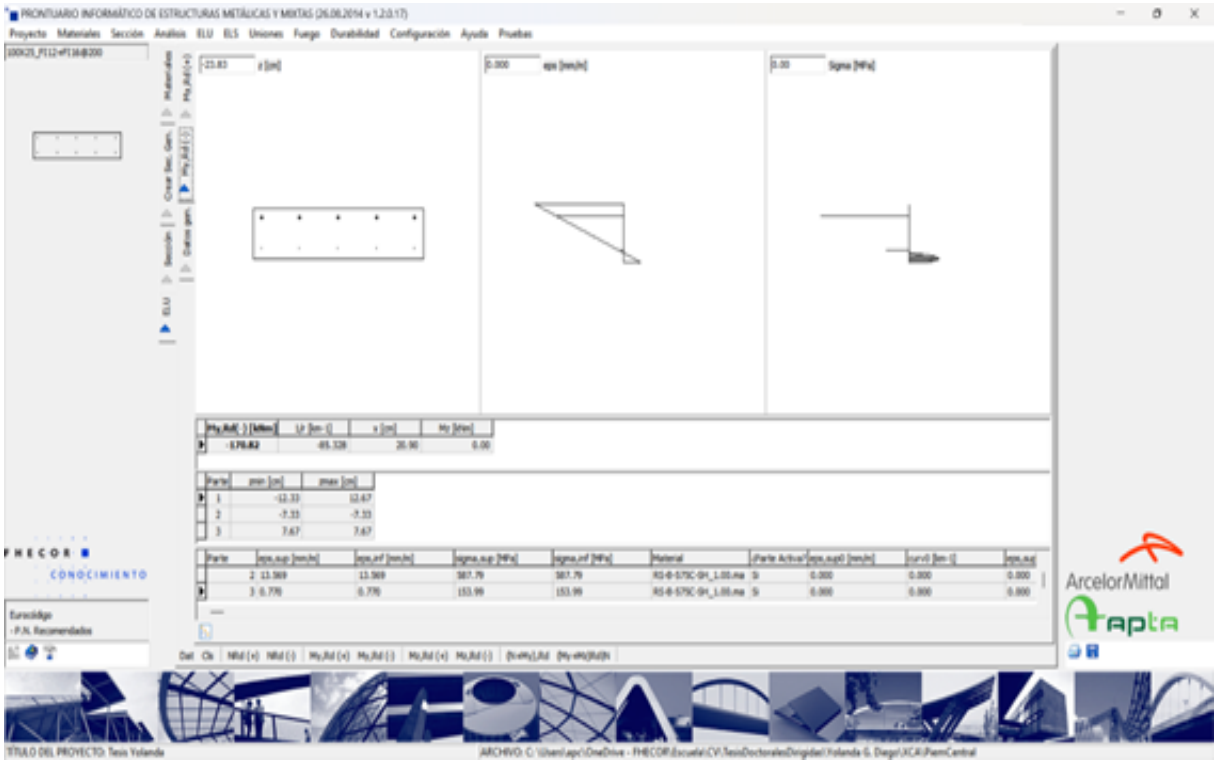

Figure 6.3: Capacity in bending of column strip section in negative bending

The ultimate bending moment without axial force for positive bending is 80 kNm, as can be seen in Figure 6.4.

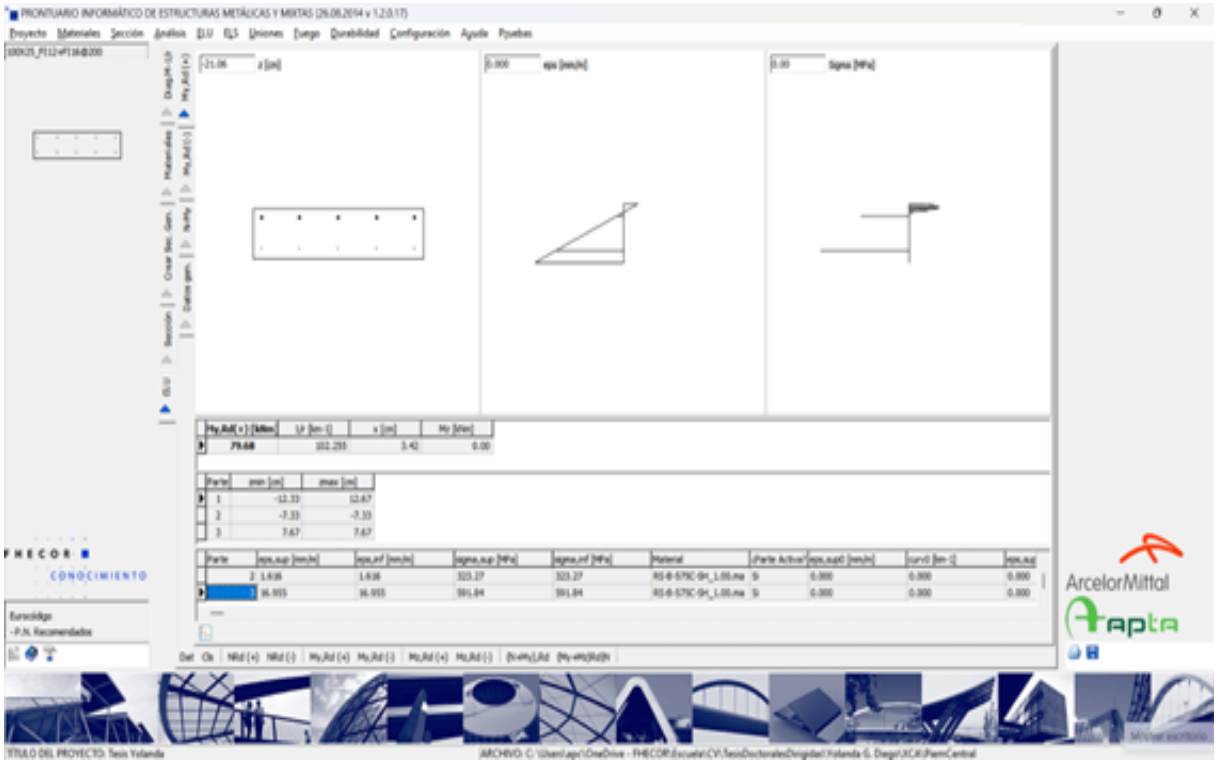

Figure 6.4: Capacity in bending of column strip section in positive bending

Figure 6.5 shows the bending moment-axial force interaction diagram, which is useful to understand how the bending capacity increases with compression and decreases with tension. All these diagrams are drafted using the mean resistance values of the materials to simulate an actual case.
The finite element model used for the analysis in this section is SOFISTIK. The change in software is prompted by ease of use. The model is a shell model which allows to automatically retrieve membrane forces and moments.

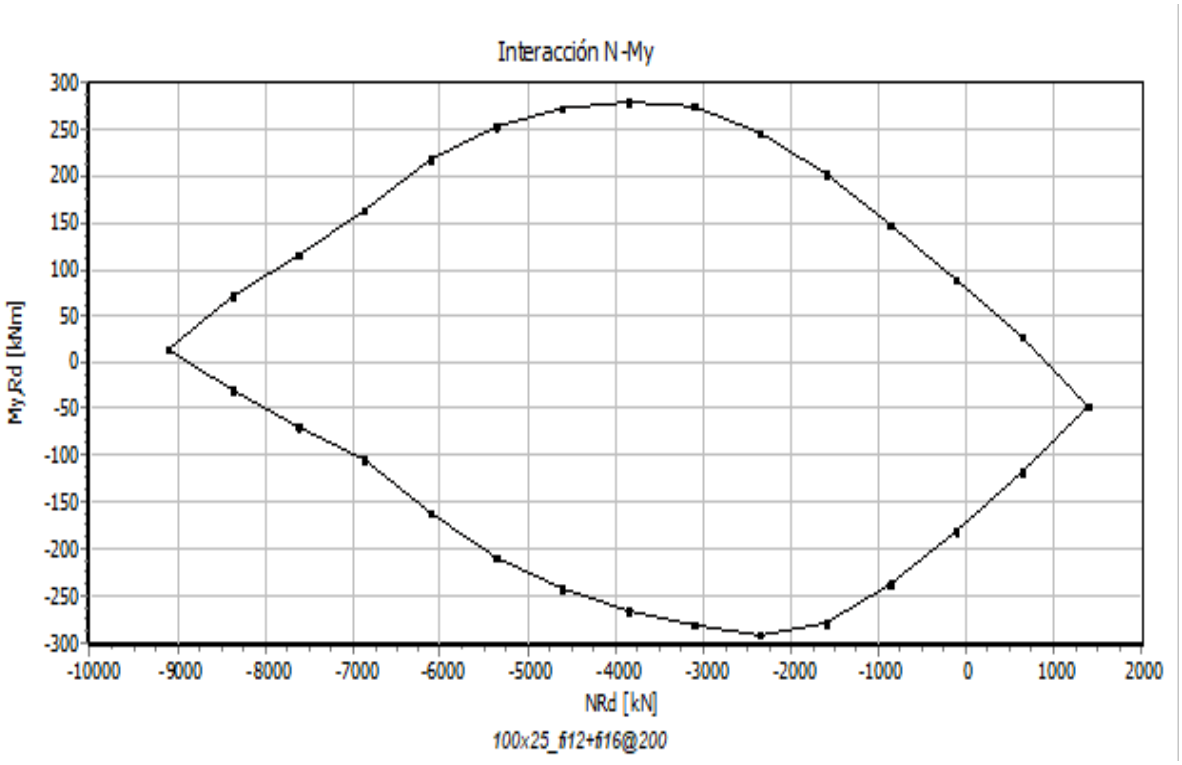

Figure 6.5: Moment-axial force interaction diagram

6.3 Model results

6.3.1 Central Column

6.3.1.1 Deflections

Deflections are sensitive to modelling, so these results should not be taken as accurate estimates of deflections occurring in real structures, but they do provide an order of magnitude. Figure 6.6 shows a view of the deformed shape of the slab after the collapse of the central column and the degree of utilization of the structure. It is apparent that the most utilized zones of the structure are those surrounding the edge columns.

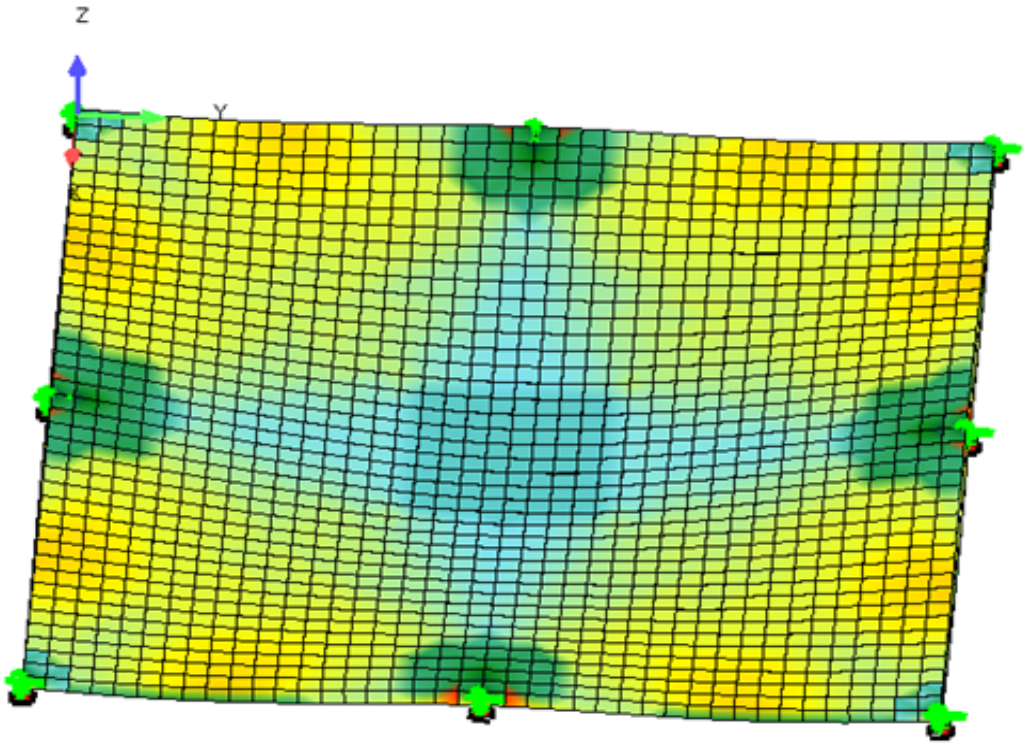

Figure 6.6: Deformed shape of the slab after collapse of the central support

Figure 6.7 shows the deflection as a function of the applied load. In the range studied the behaviour is mainly linear (except for cracking of concrete). This is explained below by the action of membrane forces, which allows the sum of bending forces to remain basically constant, so that the increase in external bending is taken by the membrane effect, without the need for yielding of reinforcement and redistribution of bending forces.

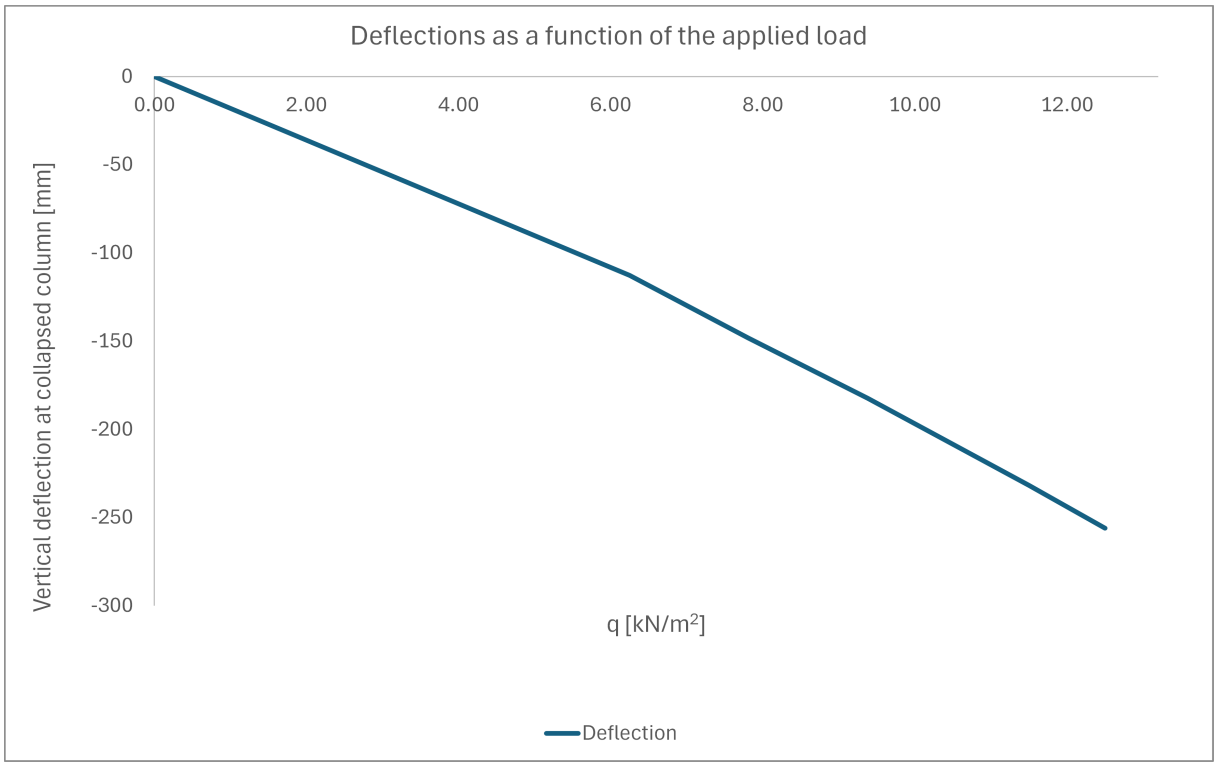

Figure 6.7: Deflections as a function of the applied load

This is explained below by the action of membrane forces, which allows the sum of bending forces to remain basically constant, so that the increase in external bending is taken by the membrane effect, without the need for yielding of reinforcement and redistribution of bending forces.

6.3.2 Forces and resistance mechanism

Figure 6.8 shows the law of membrane forces along a section by one of the slab mid-planes, passing though th location of the collapsed column (which would be at the centre of the figure). The positive and negative areas cancel each other out, with the difference of the small shear force carried by the perimetral supports, as should be the case due to equilibrium conditions. Clearly, the membrane forces increase as the load increases.

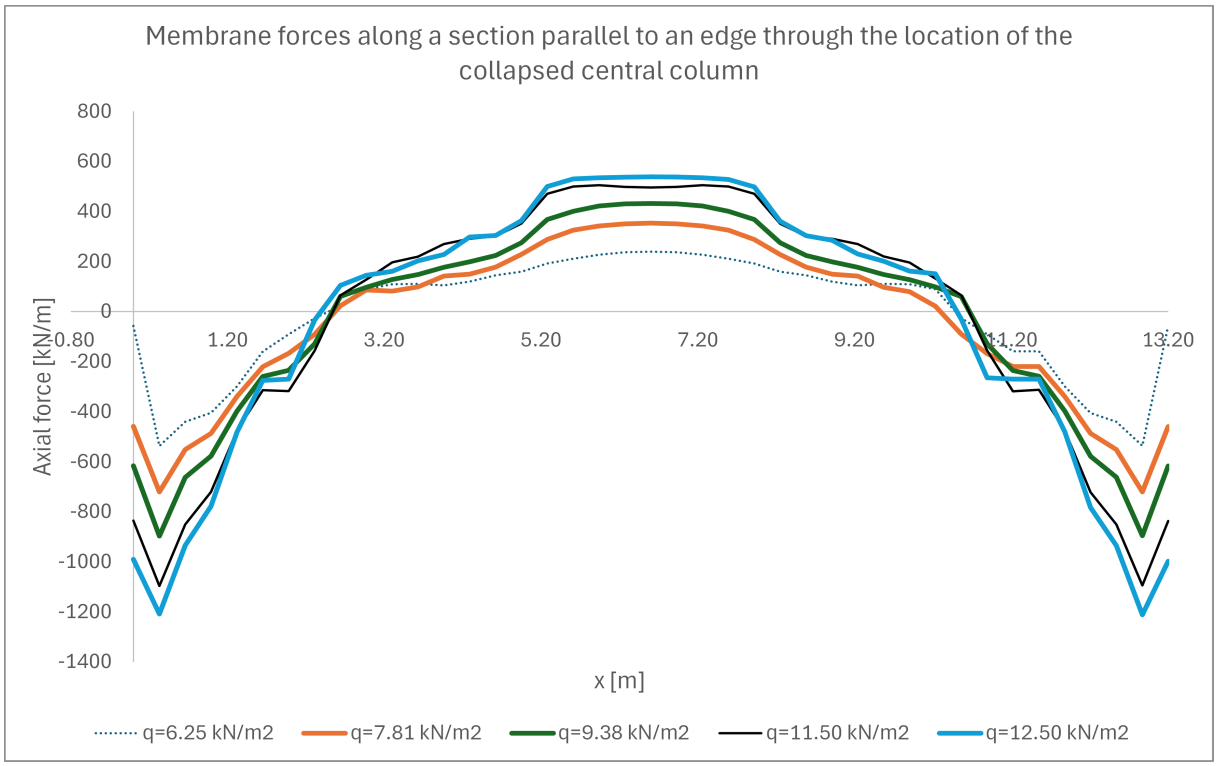

Figure 6.8: Membrane forces along section by mid-slab

In Figure 6.9 the bending moments along a cut parallel to an edge through the section of the collapsed central column are plotted for the different load levels. As the load increases, the positive bending moment in the central zone decreases, because the flexural moments are resisted by the development of membrane forces, while the opposite happened at the edges along the column strips because the development of compression forces in this zone increases the bending capacity. In any case, the negative bending moments are below the capacity in pure bending even for the highest level of load considered.

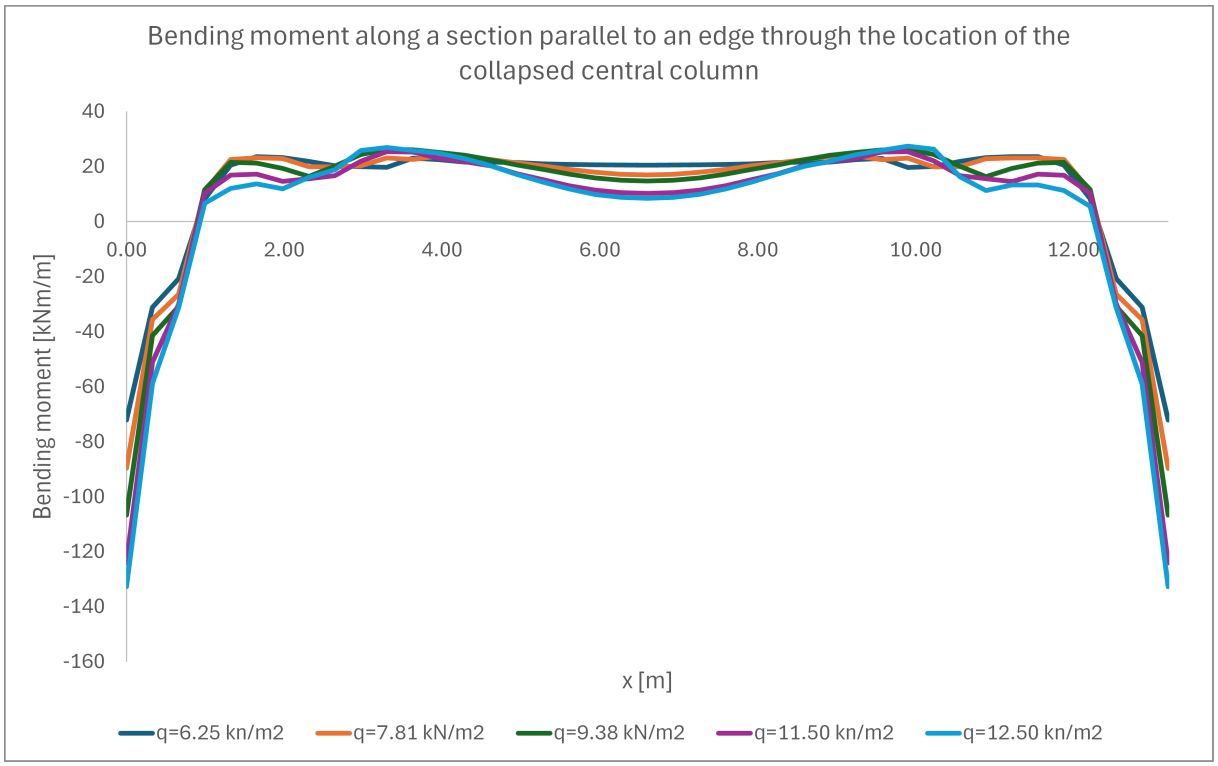

Figure 6.9: Bending moments along section by mid-slab

Figure 6.10 shows the membrane moments along the same section. The importance of membrane action is very clearly shown in this figure. For a load of 12.50 kN/m2, the positive bending moment at the centre of the slab is only 8.4 kNm/m, while the membrane moment is 45.5 kN/m, so that 84% of the bending resistance comes from membrane action.

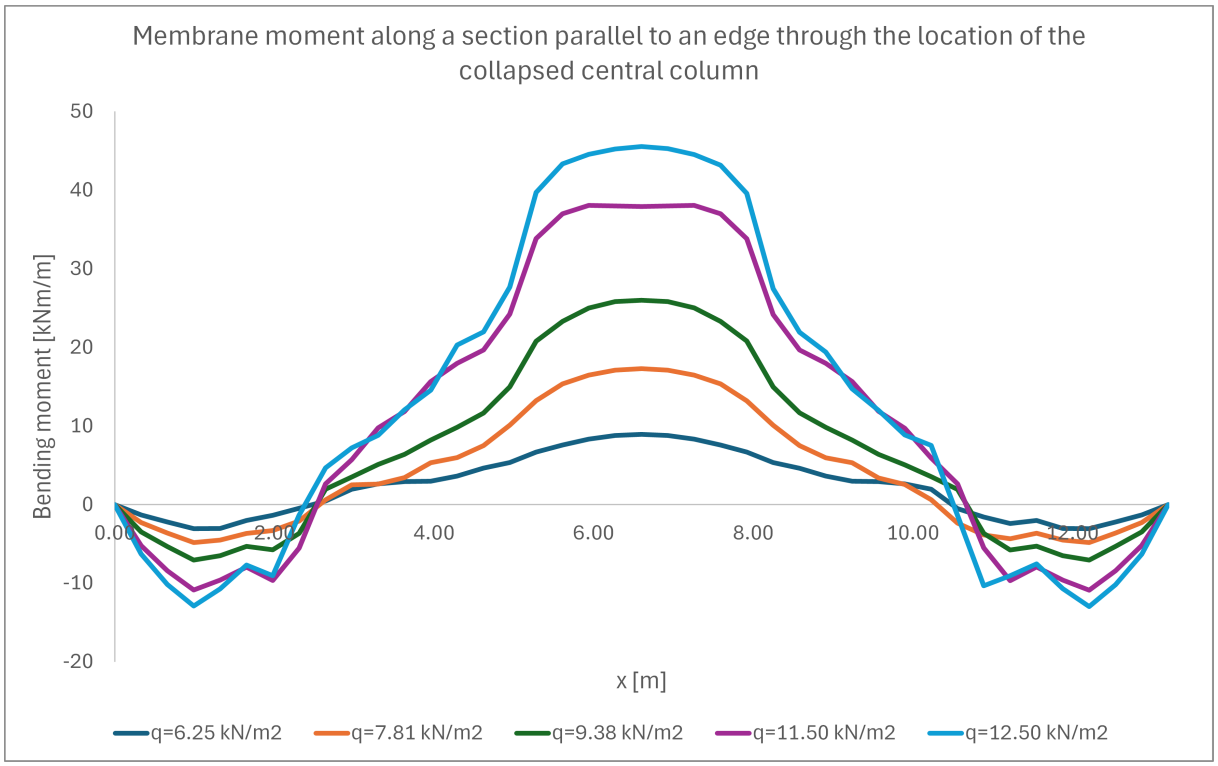

Figure 6.10: Membrane moments along section by mid-slab

The figure also shows that membrane forces are more significant in the central zone. To have a more general number regarding the importance of membrane effect, Figure 6.11 shows the algebraic sum of total moments along the section, as well as the sum of bending moments and the sum of the membrane moments.

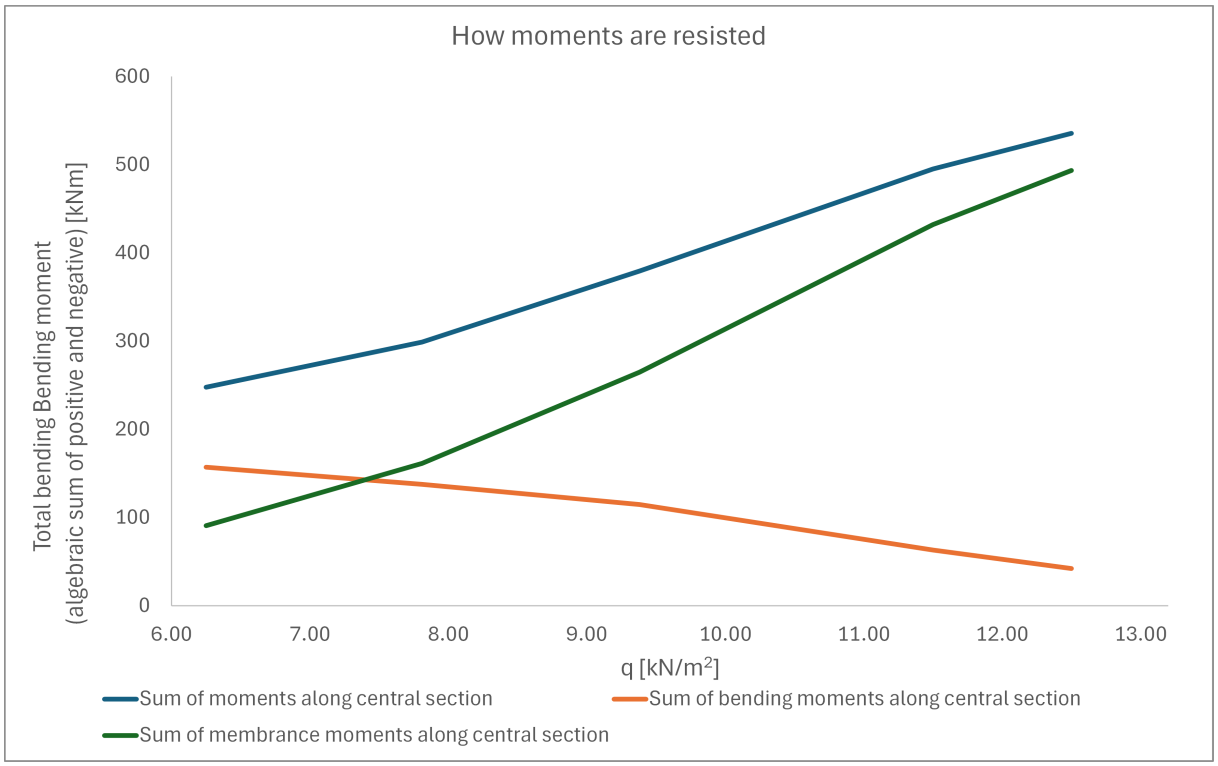

Figure 6.11: How moments are resisted (algebraic sum of positive and negative moments)

The figure shows the increased importance of the membrane effect as the applied load increases. Perhaps a better idea of this concept is provided by the absolute sum of positive and negative moments. This is represented in Figure 6.12. The absolute sum of the moments resisted by flexure remains more or less constant and the increase in moment due to increased load is taken by the membrane effect.

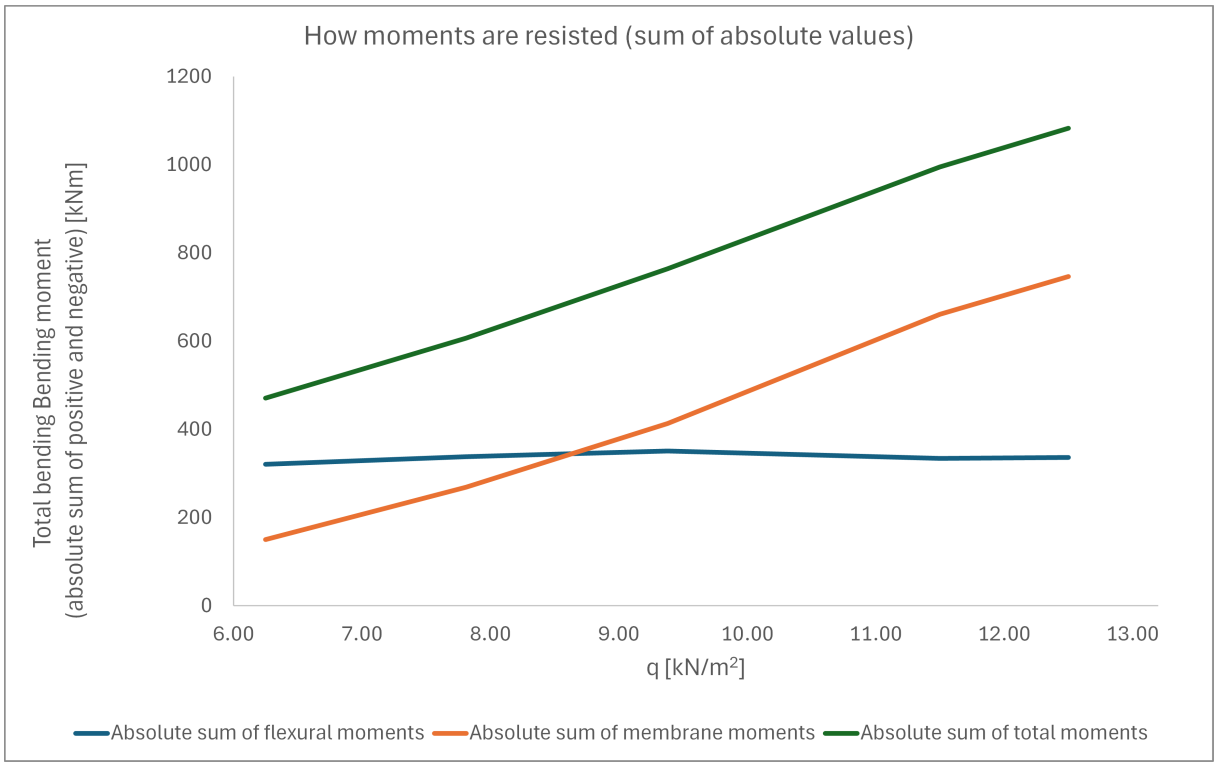

Figure 6.12: How moments are resisted (about sum of positive and negative moments)

6.3.3 Corner column

6.3.3.1 Model

For the corner column the same model described in section 6.2 is used, in which the central support is restored, and the corner support is removed. Figure 6.13 shows the top view, while Figure 6.14 shows the bottom view of the model, developed using SOFISTIK software.

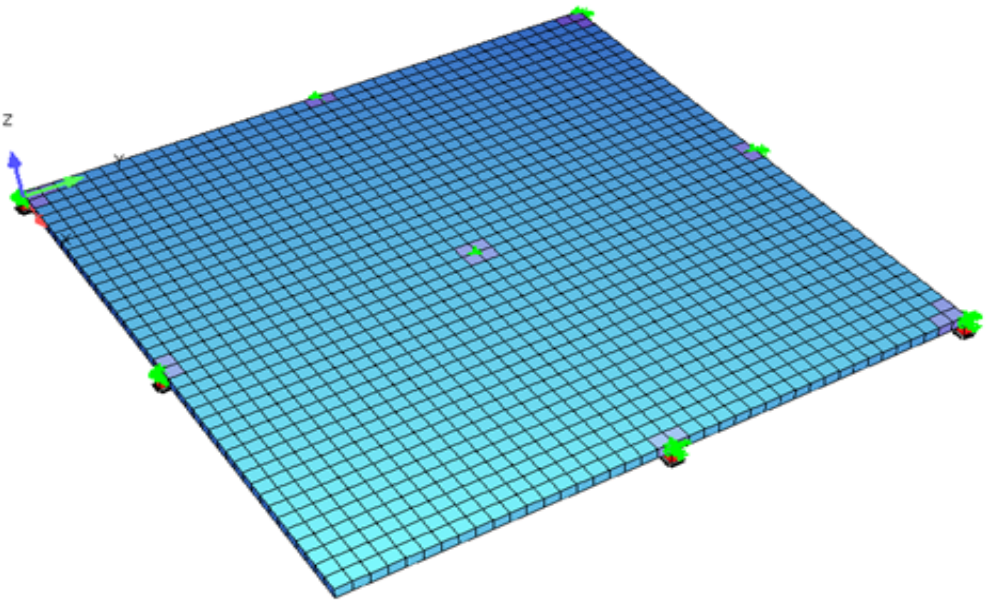

Figure 6.13: Model for the collapse of the corner column (top view)

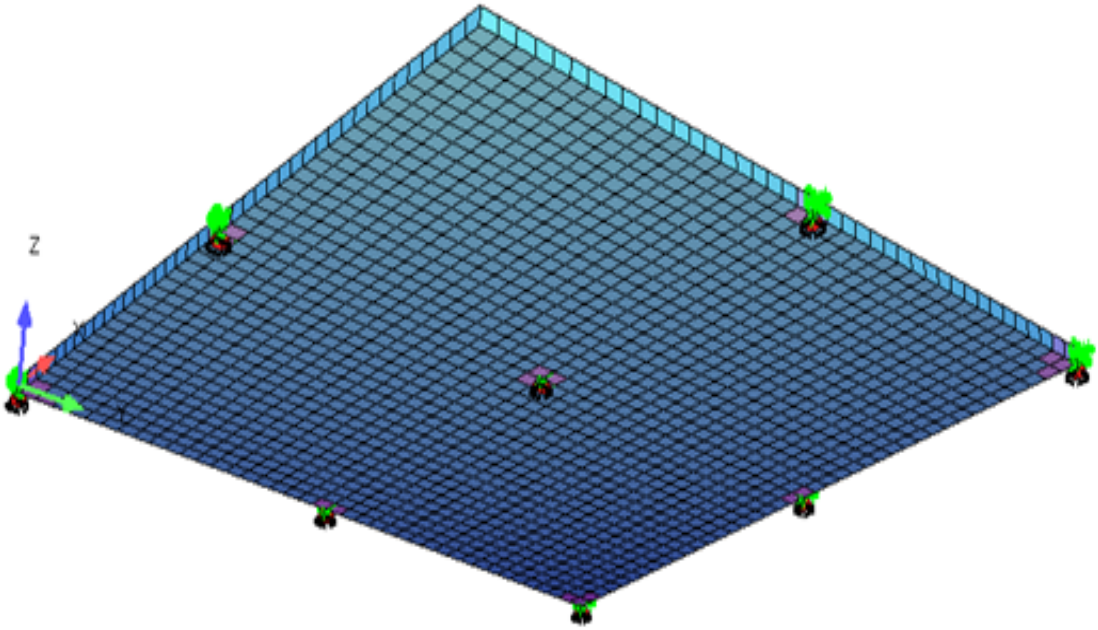

Figure 6.14: Model for the collapse of the corner column (bottom view)

6.3.3.2 Deflections

As stated above, deflections are sensitive to modelling and the values given in this section must be interpreted as orders of magnitude. Figure 6.15 shows the shape of the deformed structure, as well as the utilization ratios. It is apparent that the zones with the most stress are the areas around the two columns adjacent to the collapsed corner column and the zone around the central support.

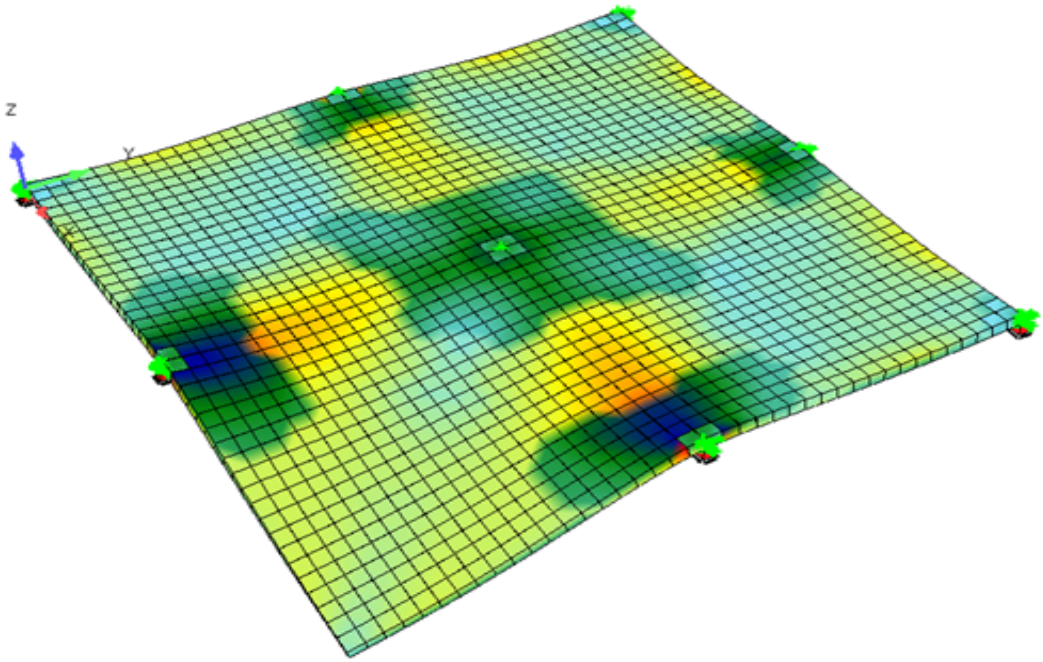

Figure 6.15: Deformed shape and utilization ratios for the case of a collapsed corner column

Figure 6.16 shows the shape of the deflected shape along the diagonal of the structure passing through the section of the collapsed column for the different loads considered.

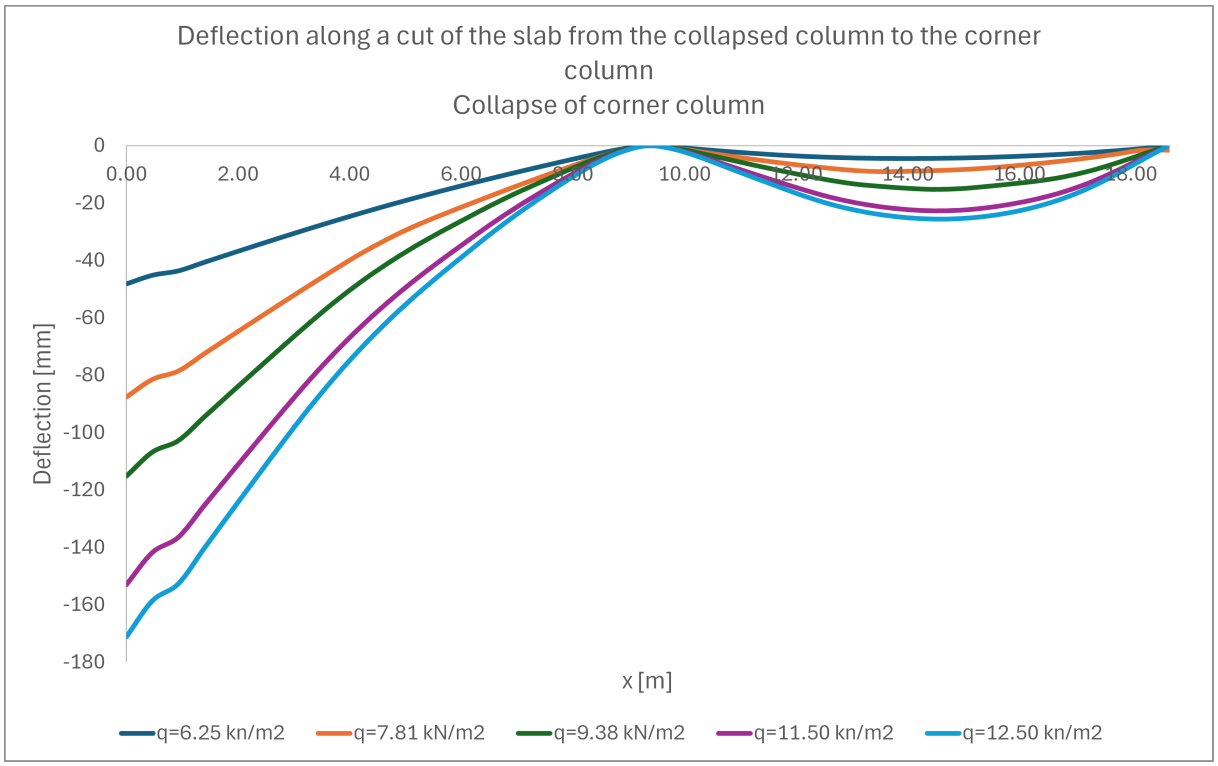

Figure 6.16: Deflections along the diagonal joining the collapsed support and the opposite corner support

6.3.3.3 Forces and resistance mechanisms

In this section the cut along a diagonal is studied. In order to obtain the forces along the cut (axial forces perpendicular to the cut and bending moments having the cut as rotation point), forces and moments in the xx, yy and xy directions need to be added vectorially. Figure 6.17 shows the sign conventions used by SOFISTIK.

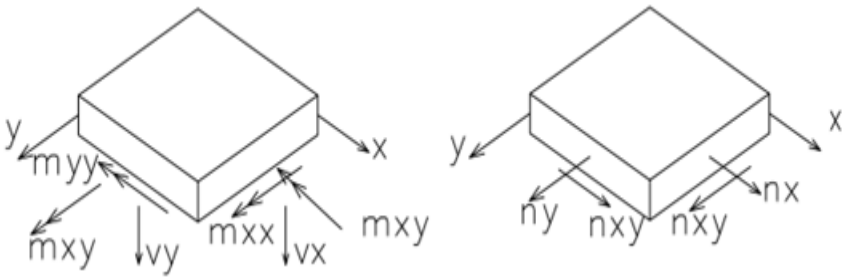

Figure 6.17: Sign conventions usesd by SOFISTIK

Therefore, the formulations used to obtain the axial forces and moments along the diagonal are as follows (l is the dimension of the finite element):

$$N = \left(\frac{(nx + ny)}{\sqrt{2}} + nxy\sqrt{2} \right) l\sqrt{2}$$
$$M = \left(\frac{(mxx + myy)}{\sqrt{2}} + mxy\sqrt{2} \right) l\sqrt{2}$$

Figure 6.18 shows the law of the axial forces perpendicular to the diagonal passing through the collapsed column. The large forces are close to the central column where the deflection is null, so these forces will not be able to supply significant membrane action. The figure also shows that the membrane forces are significant mainly in the span corresponding to the collapsed column and much smaller in the back span. Generally, membrane forces tend to increase with the increase of the load.

Figure 6.19 shows the law of the bending moments along the same diagonal. The bending moment law is quite different from that observed in the experiment carried out with single span two-storey building tested at UPM (see Section 4.2.1), where, transversely to the diagonal the bending is basically positive bending. Here, the negative being is dominant in the transversal direction because of the negative bending over the central support, which grows with the load. Positive bending is apparent, however, in the back span.
Some membrane action does develop, basically in the span of the collapsed column as shown in Figure 6.19. However, note that the absolute value of the moments generated through membrane action is quite low in this case (less than 10 kNm/m). So the picture in terms of how the forces are resisted depending on which column fails and depending on how many columns the structure has, can be very different.

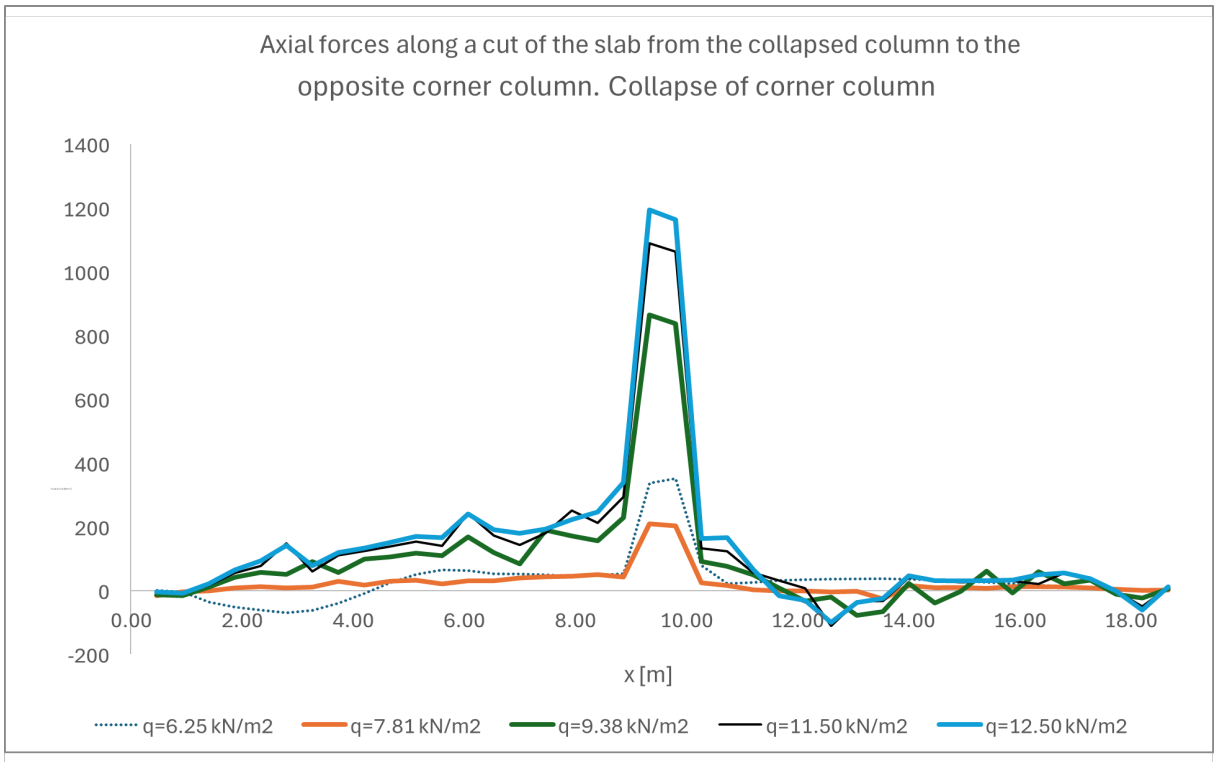

Figure 6.18: Axial forces perpendicular to the diagonal of the structure passing through the collapsed corner support

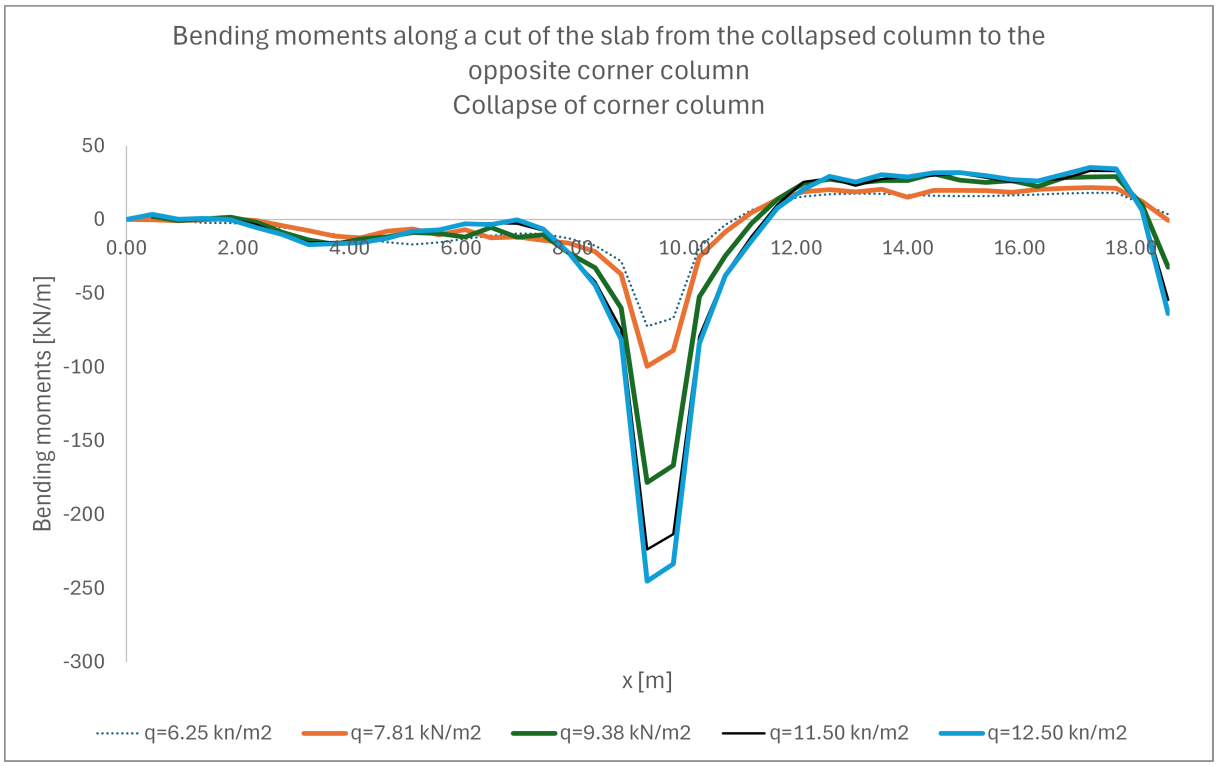

Figure 6.19: Bending moments along the diagonal of the structure passing through the collapsed corner support

Figure 6.20 shows how the bending moments resist for the case of collapse of a corner column. In this case, while there is an increase in the membrane effect with load, this effect represents less than 20% of the total moment for the highest load, while for the collapse of the central column this was 70% for the same load. This clearly shows that the membrane action is not responsible for the resistance of slabs to corner column failures. Table 6.1 shows a more detailed comparison based on the sum of the absolute values of the moments along the section.

Table 6.1 Distribution of moments between bending and membrane mechanisms for failure of a central support and a corner support

	Central support				Corner support			
q [kN/m^2]	Bending [kNm]	Membrane action [kNm]	Total bending [kNm]	% **membrane action**	Bending [kNm]	Membrane action [kNm]	Total bending [kNm]	% **membrane action**
6.25	321	150	471	**31.8%**	284.2	17.8	302.0	**5.9%**
7.81	338	269	607	**44.3%**	322.5	25.6	348.1	**7.4%**
9.38	351	413	764	**54.1%**	354.1	43.4	397.4	**10.9%**
11.5	334	661	995	**66.4%**	413.1	76.6	489.7	**15.6%**
12.5	336	746	1083	**68.9%**	440.0	93.9	534.0	**17.6%**

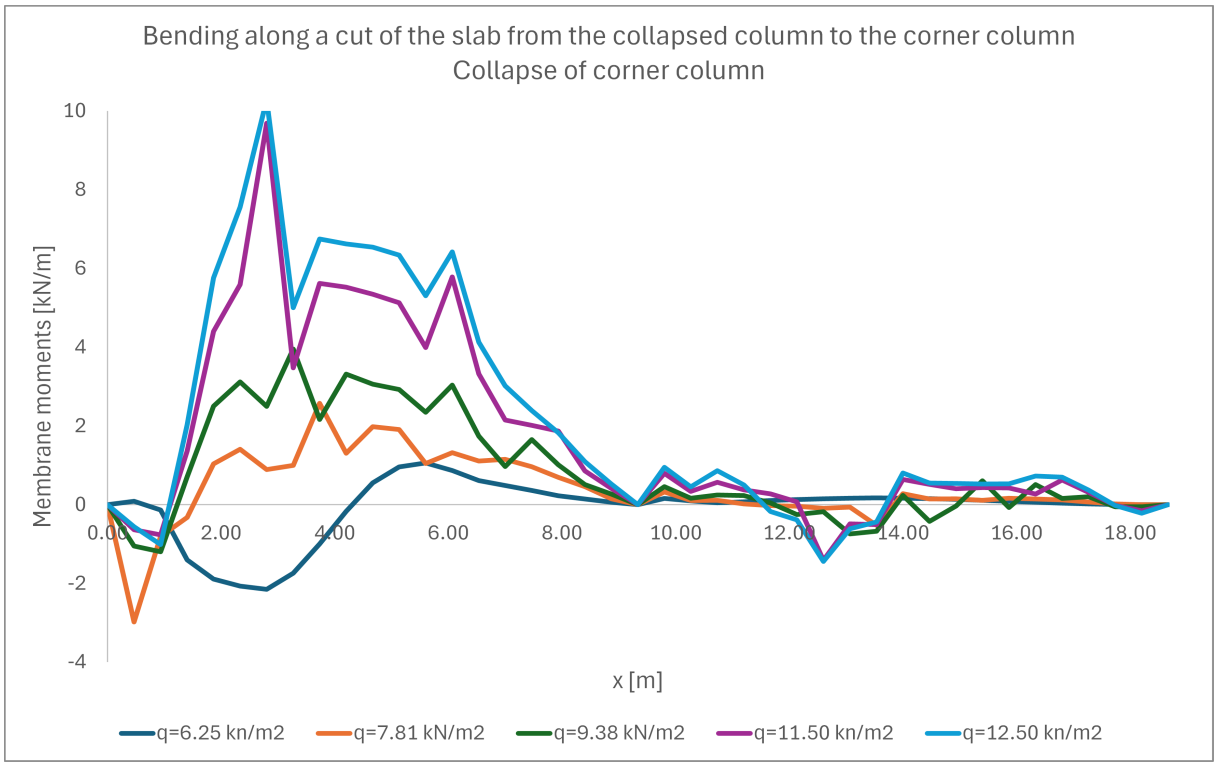

Figure 6.20: Membrane moment along the diagonal of the structure passing trough the collapsed corner support

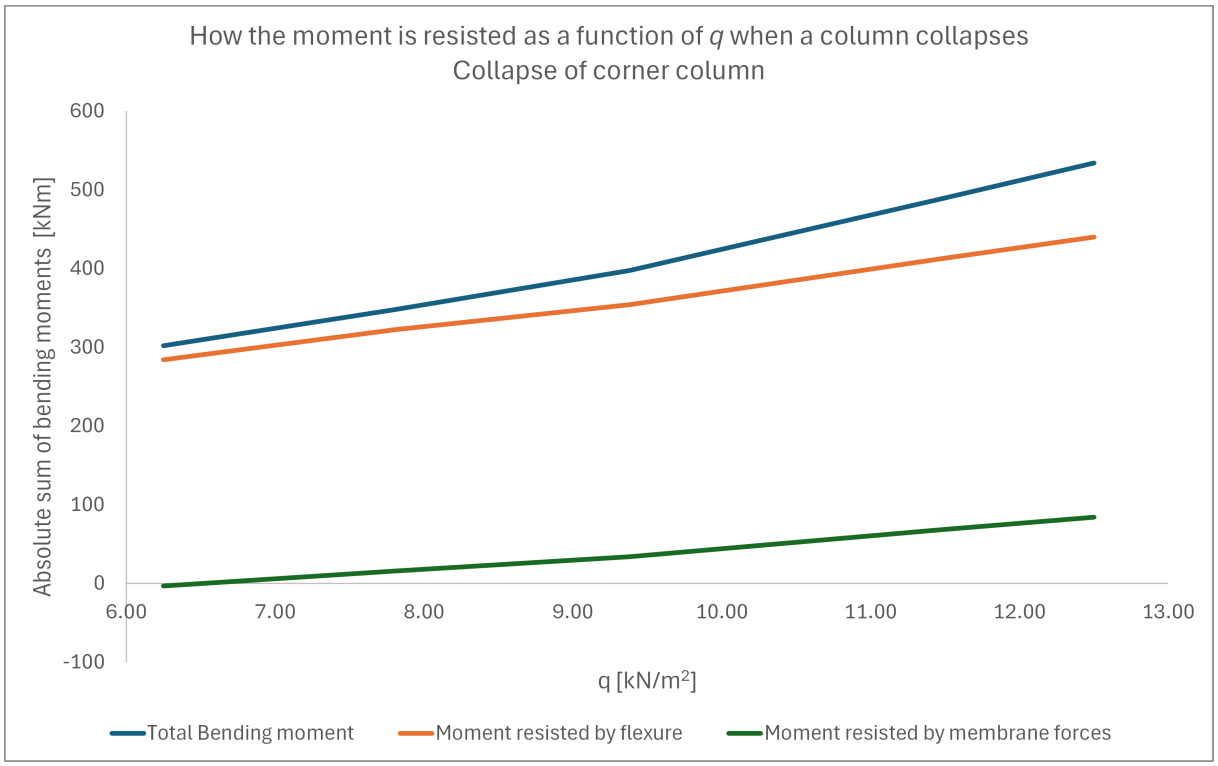

Figure 6.21: How moments are resisted (absolute sum of positive and negative moments

Chapter 7

General Conclusions and Further Research

From the different studies carried out within the framework of this thesis, the following conclusions can be drawn:

- Finite elements are a good tool to investigate the problem of robustness and can actually provide good approximations to experimental results. However, not all finite element models are equally good, and discrepancies can be found between models, especially with respect to deflections.
- Both finite elements and experimental results show that dynamic effects derived from sudden column collapse are not very significant as the measured oscillations of deflections around the equilibrium deflection are small. The problem can therefore be studied by using static calculations.
- It is not straightforward to extrapolate results from a given case to other similar cases. The importance of membrane forces is sensitive to both the type of support that collapses, as well as to the structural typologies. In the cases studied in Section 1, membrane action can go from absorbing close to 70% of all bending to less than 20%. This observation is also backed up by studies regarding the strut-and-tie models studied in Section 5.2.1.
- The study carried out shows that for structures such as those studied in this thesis (i.e. solid slabs) column collapse can be resisted without significant damage and without any need to specifically design for it for loads of twice the self-weight of the slab which is a good upper bound for most practical cases. This questions the provisions of EN 1991-1-7 Gulvanessian, 2001.

The following topics are left for future studies:

- Study of the edge support
- Study of other structural typologies such are one-way slabs, beam and slab floors, composite floors.

- Different support conditions, with less and more spans on a theoretical basis as developed in Section 1.
- Effect of the span length.
- Structures with uneven spans
- Structures with several floors

Bibliography

Adam, J. M., Buitrago, M., Bertolesi, E., Sagaseta, J., & Moragues, J. J. (2020). Dynamic performance of a real-scale reinforced concrete building test under a corner-column failure scenario. *Engineering Structures*, *210*, 110414.

Adam, J. M., Parisi, F., Sagaseta, J., & Lu, X. (2018). Research and practice on progressive collapse and robustness of building structures in the 21st century. *Engineering Structures*, *173*, 122–149.

Alañón, A., Cerro-Prada, E., Vázquez-Gallo, M. J., & Santos, A. P. (2018). Mesh size effect on finite-element modeling of blast-loaded reinforced concrete slab. *Engineering with Computers*, *34*, 649–658.

Astaneh-Asl, A., Madsen, E. A., Noble, C., Jung, R., McCallen, D. B., Hoehler, M. S., Li, W., & Hwa, R. (2001). Use of catenary cables to prevent progressive collapse of buildings. *Rep. No. UCB/CEE-Steel-2001*, *2*.

Bailey, C., & Toh, W. (2007). Behaviour of concrete floor slabs at ambient and elevated temperatures. *Fire Safety Journal*, *42*(6-7), 425–436.

Bailey, C. G. (2001). Membrane action of unrestrained lightly reinforced concrete slabs at large displacements. *Engineering Structures*, *23*(5), 470–483.

Beeby, A., & Fathibitaraf, F. (2001). Membrane effect in the reinforced concrete frames—a proposal for change in the design of frames structures. *Engineering structures*, *23*(1), 82–93.

Bermejo, M., Santos, A. P., Goicolea, J. M., & Pérez, A. (2015). Evaluación de acciones explosivas sobre estructuras de hormigón armado mediante elementos finitos. *Informes de la Construcción*, *67*(539), e095–e095.

Bi, K., Ren, W.-X., Cheng, P.-F., & Hao, H. (2015). Domino-type progressive collapse analysis of a multi-span simply-supported bridge: A case study. *Engineering Structures*, *90*, 172–182.

Byfield, M., & Paramasivam, S. (2007). The prevention of disproportionate collapse using catenary action.

Caldentey, A. P., Lavaselli, P. P., Peiretti, H. C., & Fernandez, F. A. (2013). Influence of stirrup detailing on punching shear strength of flat slabs. *Engineering Structures*, *49*, 855–865.

CEN, E., et al. (2004). 2: Design of concrete structures-part 1-1: General rules and rules for buildings. *British Standards Institution*.

Committee, A. (2008). Building code requirements for structural concrete (aci 318-08) and commentary.

Dat, P. X., & Tan, K. H. (2015). Experimental response of beam-slab substructures subject to penultimate-external column removal. *Journal of Structural Engineering*, *141*(7), 04014170.

DoD, U. (2008). Ufc 3-340-02: Structures to resist the effects of accidental explosions. *US DoD.: Washington, DC, USA*, 83.

Elkady, N., Augusthus Nelson, L., Weekes, L., Makoond, N., & Buitrago, M. (2024). Progressive collapse: Past, present, future and beyond. *Structures*, *62*, 106131.

Ellingwood, B. (2006). Mitigating risk from abnormal loads and progressive collapse. *Journal of Performance of Constructed Facilities*, *20*(4), 315–323.

EN1991:2. (2003). 1: Actions on structures-part 2: Traffic loads on bridges. *EN 1991: 2*, *6*, 2003.

Européen, C. (2004). Eurocode 2: Design of concrete structures—part 1-1: General rules and rules for buildings. *London: British Standard Institution*.

Feng, F.-F., Hwang, H.-J., Kang, S.-M., & Yi, W.-J. (2022). Multilinear model for progressive collapse response of reinforced concrete frames under penultimate column removal scenario. *Journal of Building Engineering*, *47*, 103850.

Fomento, M. (2008). Instrucción de hormigón estructural (ehe-08). *Fomento, Madrid, España*.

Frangopol, D. M., & Curley, J. P. (1987). Effects of damage and redundancy on structural reliability. *Journal of structural engineering*, *113*(7), 1533–1549.

Gouverneur, D. (2014). *Experimental and numerical analysis of tensile membrane action in reinforced concrete slabs in the framework of structural robustness* [Doctoral dissertation, Ghent University].

Gouverneur, D., Caspeele, R., & Taerwe, L. (2013). Effect of reinforcement curtailment on deflections, strain and crack development in rc slabs under catenary action. *Magazine of Concrete research*, *65*(22), 1336–1347.

Grisaro, H. Y. (2021). Effect of combined blast and fragmentation load on the dynamic response of reinforced concrete structures. *Engineering Structures*, *248*, 113244. https://doi.org/https://doi.org/10.1016/j.engstruct.2021.113244

(GSA), G. S. A. (2013). Alternate path analysis & design guidelines for progressive collapse resistance. *General Services Administration*.

Gulvanessian, H. (2001). En1991 eurocode 1: Actions on structures. *Proceedings of the institution of civil engineers-civil engineering*, *144*(6), 14–22.

Gulvanessian, H., & Vrouwenvelder, T. (2006). Robustness and the eurocodes. *Structural engineering international*, *16*(2), 167–171.

Haberland, M., & Starossek, U. (2009). Progressive collapse nomenclature. *Structures Congress 2009: Don't Mess with Structural Engineers: Expanding Our Role*, 1–10.

Hallquis, J. (2016). Ls dyna theory manual. *Livermore Software Technology Corportation*.

Hayes, B. (1968). Allowing for membrane action in the plastic analysis of rectangular reinforced concrete slabs. *Magazine of Concrete Research*, *20*(65), 205–212.

Helmy, H., Salem, H., & Mourad, S. (2012). Progressive collapse assessment of framed reinforced concrete structures according to ufc guidelines for alternative path method. *Engineering Structures*, *42*, 127–141.

Helmy, H., Salem, H., & Mourad, S. (2013). Computer-aided assessment of progressive collapse of reinforced concrete structures according to gsa code. *Journal of Performance of Constructed Facilities*, *27*(5), 529–539.

Hyde, D. (1992). Conwep, conventional weapons effects.

Johansen, K. W. (1943). *Brudlinieteorier*. I kommission hos J. Gjellerup.

Kanno, Y., & Ben-Haim, Y. (2011). Redundancy and robustness, or when is redundancy redundant? *Journal of Structural Engineering*, *137*(9), 935–945.

Keenan, W. (1969). *Strength and behavior of restrained reinforced concrete slabs under static and dynamic loadings*. Naval Civil Engineering Laboratory.

Kemp, K. (1967). Yield of a square reinforced concrete slab on simple supports, allowing for membrane forces. *The Structural Engineer*, *45*(7), 235–240.

Khoe, Y. S., & Weerheijm, J. (2012). Limitations of smeared crack models for dynamic analysis of concrete. *12th International LS-DYNA Users Conference. Constitutive Models*.

Kiakojouri, F., De Biagi, V., Chiaia, B., & Sheidaii, M. R. (2020). Progressive collapse of framed building structures: Current knowledge and future prospects. *Engineering Structures*, *206*, 110061.

Kiakojouri, F., Zeinali, E., Adam, J. M., & De Biagi, V. (2023). Experimental studies on the progressive collapse of building structures: A review and discussion on dynamic column removal techniques. *Structures*, *57*, 105059.

Kingery, C. N., & Bulmash, G. (1984). *Airblast parameters from tnt spherical air burst and hemispherical surface burst*. US Army Armament; Development Center, Ballistic Research Laboratory.

Lalkovski, N., & Starossek, U. (2014). Pancake-type collapse—preventing downward progression. *IABSE Symposium: Engineering for Progress, Nature and People, Madrid, Spain, 3-5 September 2014*, 1642–1649.

Luccioni, B., & Aráoz, G. (2011). Erosion criteria for frictional materials under blast load. *Mecánica Computacional*, *30*(21), 1809–1831.

Melo, G. S. S. d. A. (1990). *Behaviour of reinforced concrete flat slabs after local failure* [Doctoral dissertation, Polytechnic of Central London].

Merola, R. (2009). *Ductility and robustness of concrete structures under accidental and malicious load cases* [Doctoral dissertation, The University of Birmingham].

Müllers, I. (2007). *Zur robustheit im hochbau: Stützenausfall als gefährdungsbild für stahlbetontragwerke* (Vol. 304). vdf Hochschulverlag AG.

Murray, Y. D. (2004). Theory and evaluation of concrete material model 159. *8th International LS-DYNA users conference*, 25–36.

Narasimhan, H., & Faber, M. (2009). Risk assessment in engineering: Principles, system representation and risk criteria–annex: Example–assessment of structural robustness.

Nist. (2013). *Final report on the collapse of world trade center building 7, federal building and fire safety investigation of the world trade center disaster (nist ncstar 1a)*. CreateSpace Independent Publishing Platform. https://books.google.com/books?id=vMykngEACAAJ

of Civil Engineers, A. S. (2023a). Blast protection of buildings.

of Civil Engineers, A. S. (2023b). Standard for mitigation of disproportionate collapse potential in buildings and other structures.

Paramasivam, S. (2008). *Protective design against disproportionate collapse of rc and steel framed buildings* [Doctoral dissertation, University of Southampton].

Park, R. (1964). Ultimate strength of rectangular concrete slabs under short-term uniform loading with edges restrained against lateral movement. *Proceedings of the Institution of Civil Engineers*, *28*(2), 125–150.

Park, R., & Gamble, W. L. (1999). *Reinforced concrete slabs*. John Wiley & Sons.

Pham, A. T., & Tan, K. H. (2019). Analytical model for tensile membrane action in rc beam-slab structures under internal column removal. *Journal of Structural Engineering*, *145*(6), 04019040.

Pham, A. T., Tan, K. H., & Yu, J. (2017). Numerical investigations on static and dynamic responses of reinforced concrete sub-assemblages under progressive collapse. *Engineering Structures*, *149*, 2–20.

Powell, D. S. (1966). *Ultimate strength of concrete panels subjected to uniformly-distributed loads* [Doctoral dissertation].

Punton, B. (2014). *Progressive collapse mitigation using cma in rc framed buildings* [Doctoral dissertation, University of Southampton].

Qian, L., Li, Y., Diao, M., Guan, H., & Lu, X. (2020). Experimental and computational assessments of progressive collapse resistance of reinforced concrete planar frames subjected to penultimate column removal scenario. *Journal of Performance of Constructed Facilities*, *34*(3), 04020019.

Russell, J., Owen, J., & Hajirasouliha, I. (2015). Experimental investigation on the dynamic response of rc flat slabs after a sudden column loss. *Engineering Structures*, *99*, 28–41.

Sasani, M. (2008). Response of a reinforced concrete infilled-frame structure to removal of two adjacent columns. *Engineering Structures*, *30*(9), 2478–2491.

Sasani, M., Bazan, M., & Sagiroglu, S. (2007). Experimental and analytical progressive collapse evaluation of actual reinforced concrete structure. *ACI Structural Journal*, *104*(6), 731.

Sasani, M., Kazemi, A., Sagiroglu, S., & Forest, S. (2011). Progressive collapse resistance of an actual 11-story structure subjected to severe initial damage. *Journal of Structural Engineering*, *137*(9), 893–902.

Sasani, M., & Sagiroglu, S. (2008). Progressive collapse resistance of hotel san diego. *Journal of structural engineering*, *134*(3), 478–488.

Sasani, M., & Sagiroglu, S. (2010). Gravity load redistribution and progressive collapse resistance of 20-story reinforced concrete structure following loss of interior column. *ACI Structural Journal*, *107*(6), 636.

Sawczuk, A., & Winnicki, L. (1965). Plastic behavior of simply supported reinforced concrete plates at moderately large deflections. *International Journal of Solids and Structures*, *1*(1), 97–111.

Shan, L., Petrone, F., & Kunnath, S. (2019). Robustness of rc buildings to progressive collapse: Influence of building height. *Engineering Structures*, *183*, 690–701.

Smith, P., Byfield, M., & Goode, D. (2010). Building robustness research during world war ii. *Journal of Performance of Constructed Facilities*, *24*(6), 529–535.

Standard, B. (2006). Eurocode 1: Actions on structures—. *British Standard, United Kingdom*.

Starossek, U. (2007). Typology of progressive collapse. *Engineering structures*, *29*(9), 2302–2307.

Starossek, U. (2009). *Progressive collapse of structures* (Vol. 153). Thomas Telford London.

Starossek, U., & Haberland, M. (2010). Disproportionate collapse: Terminology and procedures. *Journal of performance of constructed facilities*, *24*(6), 519–528.

Tan, Z., Zhong, W.-h., Tian, L.-m., Zheng, Y.-h., Meng, B., & Duan, S.-c. (2021). Numerical study on collapse-resistant performance of multi-story composite frames under a column removal scenario. *Journal of building Engineering*, *44*, 102957.

Tanapornraweekit, G., Haritos, N., Mendis, P., & Ngo, T. (2008). Modelling of frp strengthened rc slabs subjected to blast loading. *Proceedings of the 20th Australasian Conference on the Mechanics of Structures and Materials. Toowoomba, Australia*, 419–425.

Taylor, R. (1965). A note on a possible basis for a new method of ultimate load design of reinforced concrete slabs. *Magazine of concrete research*, *17*(53), 183–186.

Teng, T.-L., Chu, Y.-A., Chang, F.-A., Shen, B.-C., & Cheng, D.-S. (2008). Development and validation of numerical model of steel fiber reinforced concrete for high-velocity impact. *Computational Materials Science*, *42*(1), 90–99.

Vecchio, F., & Tang, K. (1990). Membrane action in reinforced concrete slabs. *Canadian Journal of Civil Engineering*, *17*(5), 686–697.

Vrouwenvelder, T. (2005). Eurocode 1, part 1.7, accidental actions. *9th International Conference on Structural Safety and Reliability (ICOSSAR 2005). Rome*.

Wood, R. (1961). Plastic and elastic design of slabs and plates, with particular reference to reinforced concrete floor slabs. *London: Thames and Hudson*.

Wu, K.-C., Li, B., & Tsai, K.-C. (2011). The effects of explosive mass ratio on residual compressive capacity of contact blast damaged composite columns. *Journal of Constructional Steel Research*, *67*(4), 602–612.

Xu, K., & Lu, Y. (2006). Numerical simulation study of spallation in reinforced concrete plates subjected to blast loading. *Computers Structures*, *84*(5), 431–438. https://doi.org/https://doi.org/10.1016/j.compstruc.2005.09.029

Yi, W.-J., He, Q.-F., Xiao, Y., & Kunnath, S. K. (2008). Experimental study on progressive collapse-resistant behavior of reinforced concrete frame structures. *ACI Structural Journal*, *105*(4), 433.

Zhou, Q., & Yu, T. (2004). Use of high-efficiency energy absorbing device to arrest progressive collapse of tall building. *Journal of Engineering Mechanics*, *130*(10), 1177–1187.

Annexes

Engineering Structures 240 (2021) 112411

Contents lists available at ScienceDirect

Engineering Structures

journal homepage: www.elsevier.com/locate/engstruct

Testing robustness: A full-scale experimental test on a two-storey reinforced concrete frame with solid slabs

Alejandro Pérez Caldentey [a,b,*], Yolanda G. Diego [a], Freddy Ariñez Fernández [b], Anastasio P. Santos [a]

[a] Universidad Politécnica de Madrid (UPM), Spain
[b] FHECOR Consulting Engineers, Spain

ARTICLE INFO

Keywords:
Robustness
Column removal
Finite element modelling
Damage
Dynamic impact
Factor

ABSTRACT

This paper presents the results of a full-scale robustness test carried out on a two storey building with two square reinforced concrete slabs (25 cm deep) with a span of 6.6 m, in which a corner column was suddenly removed. Despite the extreme action, and the fact that the slab was not designed for it, only relatively minor damage was observed, with a maximum deflection around 22 cm and apparently controled cracking patterns. The slab started working as a simply supported element along the symmetry axis of the structure supported on only 3 columns. The tests was modeled using Finite Element Analysis. It was observed that the model could capture very well the behaviour of the real structure, predicting very similar cracking patterns and deflections. The structure was shored two hours after the test because deflections were not yet fully stabilized. It is suspected that this increase of deflections could be related to the deterioration by torsional effects of the connection between the slab and columns on the first floor.

1. Introduction

The modern concept of *Robustness* as currently understood in the field of structural engineering is a concept that was coined after the Ronan Point failure in 1968 [23] where a relatively small gas explosion in a buiding designed with prefabricated elements resulted in the failure of the whole corner of the building. Eurocode 1 in Part 1.7 [10] defines the concept of *Robustness* as follows:

"the ability of a structure to withstand events like fire, explosions, impact, or the consequences of human error, without being damaged to an extent disproportionate to the original cause."

Design for robustnes is dealt with in several design standards and guides. ASCE/SEI [2] establishes two direct strategies (Alternative Path Method and Specific Local Resistance Method) and one indirect strategy (Indirect Method) to avoid progressive collapse. GSA [14] develops the Alternate Path Method and includes specific requirements for reinforced concrete, structural steel, wood, masonry and cold-formed steel structures. NIST [24] provides further guidance on how to apply both direct and indirect methods as defined in ASCE/SEI-7-16. Finally, DoD [11] classifies structures according to their Risk Category and establishes minimum requirements for each category, going from tie requirements to the alternate path method to Enhanced Local Resistance for the most stringent structure category class. This publication also deals with different materials and establishes conditions for connections as well as acceptance criteria.

These methods are developed and applied to specific cases in several other publications. Among them Krauthammer [17], fosuses on the importance of connections both in steel and concrete structures. Kunnath et al. [18] provide an overview of design methods and experimental results focused mainly on the Alternate Path Method. Marjanishvili [20] elaborates on different analysis procedures to assess the risk of progressive collapse going from the simplest (linear-elastic static analysis) to the most complex (nonlinear dynamic analysis). Bao et al. [4] use macromodel techniques where joints are represented by a series of non-linear springs to simulate the behaviour of building structures subjected to sudden column removal. They successfully compare their results to refined FEM calculations for buildings designed accounting and not accounting for seismic actions. Lee et al. [19] present a simplified analysis of column removal in 2D steel frames based on assuming a trilinear Force-Rotation diagram and using energy-based principles. Brunesi et al. [5] analyse examples of 2D and 3D RC frame structures, under different column removal scenarios, using a fibre-based software implemented into Opensees and SeismoStruct and validate the calculations using LS-Dyna. Comparison to current code provisions reveal that code provisions are over-conservative. Eren et al.

* Corresponding author.

https://doi.org/10.1016/j.engstruct.2021.112411
Received 23 July 2020; Received in revised form 24 March 2021; Accepted 14 April 2021
Available online 4 May 2021

Engineering Structures 296 (2023) 116969

Contents lists available at ScienceDirect

Engineering Structures

journal homepage: www.elsevier.com/locate/engstruct

Experimental response and numerical modelling of a full-scale two-span concrete slab frame subjected to blast load

Lina M. López [a,*], Alejandro Pérez-Caldentey [b,c], Anastasio P. Santos [a], Yolanda G. Diego [b], Ricardo Castedo [a], María Chiquito [a]

[a] Universidad Politécnica de Madrid– ETSI Minas y Energía, C Ríos Rosas 21, 28003 Madrid, Spain
[b] Universidad Politécnica de Madrid – ETSI Caminos, Canales y Puertos. C. Prof Aranguren 3, 28040 Madrid, Spain
[c] FHECOR Consulting Engineers, Spain

ARTICLE INFO

Keywords:
Full-scale test
RC frame
Blast loads
Explosion
LS-DYNA

ABSTRACT

Three full scale tests have been carried out on the same structure to determine the effect produced by several blast loadings detonated at different times. The structure is a two-span 7.00 × 14.00 m^2 RC frame subjected to explosives load from 10 to 20 kg TNT equivalent at distances varying from 0.5 m to 1.5 m. The tests were monitored using pressures gauges, accelerometers, high-speed camera and a 3D topography scanner for measurement of permanent deflections. The test results show the robustness of the slab, with only minor cracking damage in the first two loading scenarios and only local damage in the third scenario, where the equivalent load of 20 kg TNT is placed only 50 cm from the slab surface. The third test produced maximum deflections of about 4 cm and a local punching failure measuring 66 cm in diameter on the upper face and 82 cm in diameter on the lower face. The simulation of the building was carried out with the LS-DYNA software with a Lagrangian formulation for the walls, using the Load Blast Enhanced (based on CONWEP) module. Permanent defections and damage has been evaluated and has been compared with numerical modelling.

1. Introduction

The tests which are documented and analyzed in this paper were carried out within the framework of research project ITSAFE, a project partially funded by the Spanish Government and the European Union (reference number IPT-2012-0845-370000) and uniting a Consortium integrated by DRAGADOS, FHECOR and the Technical University of Madrid (UPM), whose purpose was to develop a methodology to assess the blast vulnerability of existing large transportation facilities and make recommendations for design of future infrastructures, considering this very important safety issue. The project is focused specifically on the risk of moderate weight explosive devices (up to 20 kg of TNT equivalent) which can be introduced into transportation facilities where access control is not viable. It is aimed at helping safety officials, in charge of large infrastructure buildings, manage situations involving explosive load threats especially where the need for user mobility limits the capacity to carry out security checks. For this, an estimate of the effect of a given load scenario on a given structure, is of great help in making decisions involving, for instance, what part of a large building should be evacuated. The lack of full-size tests places the weight of establishing protocols for given potential situations on finite element simulations [1–3], which are excellent at modelling known results but can be very poor at predicting the behaviour beforehand. It was considered worth it to obtain the experimental data in order to better understand how a structure would be damaged.

From the initial vulnerability studies carried out within the framework of the project, it was concluded that, for floors, the structural typology best adapted for blast load resistance is a solid reinforced or prestressed concrete slab. In order to test the robustness of existing buildings, involving this floor typology, a realistic structure to be tested under blast load was designed using traditional design methods as is fully described in this paper. Robustness is defined in EN 1991-1-7 [4] as "the ability of a structure to withstand events like fire, explosions, impact or frequency of an occurrence of a defined hazard, without being damaged to an extent disproportionate to the original clause". Following this definition, the loads are placed so as to maximize damage in the slab. Within the framework of the ITSAFE project, damage, or failure of supports was studied in parallel robustness tests which are documented

* Corresponding author.
E-mail address: lina.lopez@upm.es (L.M. López).

https://doi.org/10.1016/j.engstruct.2023.116969
Received 1 March 2023; Received in revised form 30 August 2023; Accepted 24 September 2023
Available online 30 September 2023

buildings

MDPI

Article

Robustness of Reinforced Concrete Slab Structures: Lessons Learned from Two Full-Scale Tests

Alejandro Pérez Caldentey [1,*], Yolanda G. Diego [2], Anastasio P. Santos [3], Lina López [3], María Chiquito [3] and Ricardo Castedo [3]

[1] FHECOR North America, ETSI Caminos, Canales y Puertos, Universidad Politécnica de Madrid, Prof. Aranguren 3, 28040 Madrid, Spain
[2] ETSI Caminos, Canales y Puertos, Universidad Politécnica de Madrid, Prof. Aranguren 3, 28040 Madrid, Spain; yolanda.gdiego@alumnos.upm.es
[3] ETSI de Minas y Energía, Universidad Politécnica de Madrid, C. de Ríos Rosas, 21, 28003 Madrid, Spain; tasio.santos@upm.es (A.P.S.); lina.lopez@upm.es (L.L.); maria.chiquito@upm.es (M.C.); ricardo.castedo@upm.es (R.C.)
* Correspondence: apc@fhecor.es

Abstract: Within the research project ITSAFE, two full-scale structures were built, one consisting of a single-storey, two-span, 7.00 × 14.00 m^2 RC frame with a solid slab and another consisting of a two-storey, 7.00 × 7.00 m^2 RC frame with solid slabs. In the two-span frame, one of the central supports was first demolished using a pneumatic hammer, resulting in rather limited damage (a 14–15 cm deflection at the removed support location). However, torsional cracks appeared at the interface between a column and slab in one of the outer supports. When the second central support was removed, the structure collapsed with the failure of the support–slab connection. The same type of cracking was observed in the two-storey structure, where the column removal was dynamic, and a 22 cm deflection was measured. These experimental results question current practice in which, for internal supports, alternative load path mobilizing membrane forces in the slab are said to prevent their collapse, or in the cases of edge and corner columns, rupture line analysis is used and suggests that special reinforcement at the column–support connection is also needed to prevent the premature failure of the structure.

Keywords: robustness; column removal; support–slab connection; torsion; edge support; corner support; strut-and-tie models; rupture line analysis

Citation: Pérez Caldentey, A.; G. Diego, Y.; Santos, A.P.; López, L.; Chiquito, M.; Castedo, R. Robustness of Reinforced Concrete Slab Structures: Lessons Learned from Two Full-Scale Tests. *Buildings* **2024**, *14*, 558. https://doi.org/10.3390/buildings14020558

Academic Editor: Rajai Zuheir Al-Rousan

Received: 24 January 2024
Revised: 11 February 2024
Accepted: 14 February 2024
Published: 19 February 2024

1. Introduction

Robustness is an increasing concern in today's society, with the demand to avoid structural damage unproportional to the cause becoming a standard requirement when designing structures. EN 1991-1-7 [1] and ASCE/SEI 7-16 [2] propose different strategies for designing with robustness and achieving this goal. One of the main strategies is to provide structures with an alternate load path, normally based on mobilizing membrane forces within the floors, to avoid structural collapse as a consequence of column collapse. Such alternate load path analyses can lead to very high theoretical load capacities.

From the experience obtained from the results of two full-scale tests performed within the research project ITSAFE and further analyses based on these examples, it has become clear, however, that while the provision of alternate load paths for internal columns and rupture line analyses for corner and edge columns are viable solutions, they must be complemented with special detailing of the column–slab connection. Otherwise, premature failure could be observed.

Even though there have been a number of robustness tests carried out on reduced-scale models [3–6], there are very few real-scale tests involving sudden column removal.

6th International Conference on Protective Structures (ICPS6)
14 – 17 May 2023, Auburn University USA

FULL-SCALE TEST OF TWO-SPAN CONCRETE FRAME SUBJECTED TO SUCCESSIVE BLAST LOADS

Lina M. Lopez
Universidad Politécnica de Madrid, ETSI de Minas y Energía, C. de Ríos Rosas, 21, 28003 Madrid,
lina.lopez@upm.es (corresponding autor)
Alejandro Pérez Caldentey
FHECOR North America, Universidad Politécnica de Madrid, ETSI Caminos, Canales y Puertos, Prof Aranguren 3, 28040 Madrid, Spain , apc@fhecor.es
Anatasio P. Santos, Ricardo Castedo, Maria Chiquito
Universidad Politécnica de Madrid, ETSI de Minas y Energía, C. de Ríos Rosas, 21, 28003 Madrid,
tasio.santos@upm.es, ricardo.castedo@upm.es, maría.chiquito@upm.es,
Yolanda G. Diego
Universidad Politécnica de Madrid, ETSI Caminos, Canales y Puertos, Prof Aranguren 3, 28040 Madrid, Spain
yolanda.gdiego@alumnos.upm.es

ABSTRACT

The behavior of a full-scale reinforced concrete structure was studied against successive explosive charges. Three tests have been carried out on the same structure to determine the effect produced by several blast loadings detonated at different times. The structure is a two-span 7.00×14.00 m^2 RC frame subjected to explosives load from 10 to 20 kg TNT equivalent. Pressures and accelerations were recorded at various locations on the slab to characterize the explosion and the response of the structure. The pressures recorded range from 50 to 475 kPa and the accelerations from -189 to 182 g. During the tests, high-speed videos were recorded, allowing the evolution of the fireball and the shock wave to be observed during each test. The permanent deflections produced in the slab of the structure were recorded using a 3D scanner and a laser distance meter at a series of pre-marked points forming a relatively dense mesh. The third test, carried out with 20 kg of explosive on the upper floor, produced maximum deflections of about 4 cm and a local punching failure measuring 66 cm in diameter on the upper face and 82 cm in diameter on the lower face. Damage has been evaluated and has been compared with a FEM model using LSDYNA.

Keywords: Full-scale test, RC frame, Damage, Blast loads

ROBUSTNESS OF RC STRUCTURES: CONCLUSIONS FROM TWO FULL-SCALE TESTS AND THEIR ANALYSIS

Alejandro Pérez Caldentey
FHECOR North America, Universidad Politécnica de Madrid, ETSI Caminos, Canales y Puertos, Prof Aranguren 3, 28040 Madrid, Spain
apc@fhecor.es

Yolanda G. Diego
Universidad Politécnica de Madrid, ETSI Caminos, Canales y Puertos, Prof Aranguren 3, 28040 Madrid, Spain
yolanda.gdiego@alumnos.upm.es

Anastasio P. Santos, Lina López, María Chiquito, Ricardo Castedo
Universidad Politécnica de Madrid, ETSI de Minas y Energía, C. de Ríos Rosas, 21, 28003 Madrid,
tasio.santos@upm.es, lina.lopez@upm.es, maría.chiquito@upm.es, ricardo.castedo@upm.es

ABSTRACT
Within research project ITSAFE, partially funded by the Spanish Government (Project Code: IPT-2012-0845-370000), two full-scale structures were built, one consisting of a single story two-span 7.00×14.00 m² RC frame with a solid slab and another one consisting of a two-story 7.00x7.00 m² frame also of RC with solid slabs. In the two-span frame, one of the central supports was first demolished using a pneumatic hammer resulting in rather limited damage (a 14-15 cm deflection at the removed support location). However torsional cracks appeared at the interface between column and slab at one of the outer supports. When the second central support was removed the structure collapsed due to failure of the support-slab connection. The same type of cracking was observed in the two-story structure, where the column removal was dynamic, and a 22 cm deflection was measured. These experimental results put question current practice where an alternative load-path mobilizing membrane forces in the slab is said to prevent collapse and suggests that special reinforcement at the column-support connection is also needed to prevent premature failure of the structure.

Keywords: Robustness, Column-removal, Support-slab connection, Torsion

1 Introduction

Robustness is an increasing concern in today's society with the demand to avoid structural damage unproportional to the cause becoming a standard requirement when designing structures. EN 1991-1-7 [1] and ASCE/SEI 7-16 [2] propose different strategies to design for robustness and achieve this goal. One of the main strategies is to provide the structures with an alternate load path, normally based on mobilizing membrane forces within the floors to avoid structural collapse as a consequence of column collapse. Such alternate load path analyses can lead to very high theoretical load capacities.

From the experience obtained from the results of two full-scale tests performed within research project ITSAFE, and further analyses based on these examples, it has become clear, however, that while the